J. Physiol. (1982), **330**, *pp.* 537–572
With 25 text-figures
Printed in Great Britain

M-CURRENTS AND OTHER POTASSIUM CURRENTS IN BULLFROG SYMPATHETIC NEURONES

BY P. R. ADAMS*, D. A. BROWN† AND A. CONSTANTI†

From the Department of Physiology and Biophysics, University of Texas Medical Branch, Galveston, TX 77550, U.S.A.

(*Received 4 January 1982*)

SUMMARY

1. Bullfrog lumbar sympathetic neurones were voltage-clamped *in vitro* through twin micro-electrodes. Four different outward (K^+) currents could be identified: (i) a large sustained voltage-sensitive delayed rectifier current (I_K) activated at membrane potentials more positive than −25 mV; (ii) a calcium-dependent sustained outward current (I_C) activated at similar positive potentials and peaking at +20 to +60 mV; (iii) a transient current (I_A) activated at membrane potentials more positive than −60 mV after a hyperpolarizing pre-pulse, but which was rapidly and totally inactivated at all potentials within its activation range; and (iv) a new K^+ current, the M-current (I_M).

2. I_M was detected as a non-inactivating current with a threshold at −60 mV. The underlying conductance G_M showed a sigmoidal activation curve between −60 and −10 mV, with half-activation at −35 mV and a maximal value ($\bar{G}_M$) of 84 ± 14 (S.E.M.) nS per neurone. The voltage sensitivity of G_M could be expressed in terms of a simple Boltzmann distribution for a single multivalent gating particle.

3. I_M activated and de-activated along an exponential time course with a time constant uniquely dependent upon voltage, maximizing at ≃ 150 ms at −35 mV at 22 °C.

4. Instantaneous current–voltage (I/V) curves were approximately linear in the presence of I_M, suggesting that the M-channels do not show appreciable rectification. However, the time- and voltage-dependent opening of the M-channels induced considerable rectification in the steady-state I/V curves recorded under both voltage-clamp and current-clamp modes between −60 and −25 mV. Both time- and voltage-dependent rectification in the voltage responses to current injection over this range could be predicted from the kinetic properties of I_M.

5. It is suggested that I_M exerts a strong potential-clamping effect on the behaviour of these neurones at membrane potentials subthreshold to excitation.

* Present address: Department of Neurobiology, State University of New York, Stonybrook, NY 11790, U.S.A.

† Present address: Department of Pharmacology, The School of Pharmacy, University of London, 29/39 Brunswick Square, London, WC1N 1AX.

INTRODUCTION

The present experiments arose from an inquiry into the mechanism whereby activation of muscarinic receptors depolarizes sympathetic ganglion cells. In voltage-clamped bullfrog sympathetic neurones we found that the principal effect of muscarinic agonists is to suppress a time- and voltage-dependent K^+ current, which we have provisionally termed the M-current (I_M: Brown & Adams, 1979, 1980). In this paper we describe the kinetic properties of I_M and show how it differs from other K^+ currents in bullfrog neurones.

METHODS

Preparation. Both paravertebral ganglionic chains were removed from large bullfrogs (*Rana catesbiana*). Usually one chain was refrigerated in frog Ringer to be used the following day, while the other was separated into ganglia which were pinned out on the Sylgard base of a small Perspex chamber. Mostly the two large most-caudal ganglia were used. The ganglia were cleaned of connective tissues as far as possible, and then usually treated with 10% trypsin (Sigma type 1) solution for 10–15 min. Further cleaning and repinning followed this trypsinization. The advantages of trypsin were (1) that the cells were much easier to see, and (2) that they were easier to penetrate. Sufficient experiments were completed in non-trypsinized ganglia to show that the outward currents described in this paper were not materially affected by trypsin. Possible other effects of trypsinization are considered under Results. The preparation was illuminated from below by a fibre-optic light pipe (Dolan Jenner), and viewed with a Wild M5A stereomicroscope (20 × eyepieces). Though cellular details could not be discerned, the global view of the ganglia afforded by this instrument was very useful in picking out the largest cells, from which most of the data were collected. Though no determinations of conduction velocity was made, we suppose that only the 'B' type cells were studied (cf. Nishi, Soeda & Koketsu, 1965; Tosaka, Chichubu & Libet, 1968; Weitsen & Weight, 1977), in view of their large size; and, on occasions when the preganglionic chain was stimulated (Adams & Brown, 1980, and personal observations), only the fast and slow excitatory post-synaptic potentials were observed without the intervening slow inhibitory post-synaptic potential characteristic of C cells (Tosaka *et al.* 1968). However, experiments using a single micro-electrode voltage-clamp method (not included in the present description), in which a wider range of neurones were impaled, indicated that the M-current is not restricted to the largest cells, and J. P. Horn & J. Dodd (personal communication) have detected the presence of I_M in identified C cells.

Solutions. Standard Ringer solution contained 115 mM-Na, 2 mM-Ca, 10 mM-Mg, 129 mM-Cl and 2–5 mM-Tris, adjusted to pH 7·2 with HCl. The effects of deviating from this composition, if any, are described under Results.

Solutions were led into the bath by gravity from one of two reservoirs, and then aspirated. The flow rate was 1·0–0·2 ml s^{-1}. Four electronically controlled solenoid valves (General Valve Corporation) were mounted close to the chamber in such a way as to allow remote control of the following operations: on/off of flow; switching between reservoirs; draining of either reservoir and its associated tubing. All experiments were conducted at 22 °C.

Micro-electrodes. Our standard micro-electrodes were pulled using 1·5 mm o.d. fibre-filled tubing (WP Instruments) on a horizontal puller (Industrial Science Associates), to give resistances of 40–80 MΩ when filled with 3 M-KCl. Although these electrodes were sometimes usable in their original state, we encountered three types of problem: slow clamp due to high resistance; uncertain resting potentials; and spontaneous blocking of the electrodes while in the cell. All three problems could be alleviated by breaking back the tips to resistances in the 20–40 MΩ range, by tapping them gently on the bottom of the experimental chamber. Such broken electrodes seemed to give much better results than electrodes initially pulled to a low resistance.

Electrical recording. The micro-electrodes were connected to WPI head-stages via WPI electrode holders, the metal pins of which were bent to give an impalement angle about 15° from the vertical. The WPI head-stages were carried on C. Z. Jena sliding plate manipulators, and the electrodes inserted under visual control into the same cell. Impalement was usually achieved by lowering the

electrode tip onto the cell surface, applying a little pressure, and then briefly over-compensating the negative capacity adjustment. Over-compensation was achieved by modifying the WPI circuitry ('zap' modification suggested by R. Nicoll). Foot-switches allowed 'zapping' while leaving the hands free for manipulation.

The current-passing electrode was used in conjunction with a WPI M701 bridge preamplifier. The addition of a WPI 'breakaway box' allowed the electrode and head-stage to be disconnected from the preamplifier, and connected instead to the output of the voltage clamp amplifier.

The voltage recording electrode was connected to one headstage of the WPI M777 differential electrometer. The other headstage was connected to an AgCl pellet bath reference electrode. The unity gain differential output of the WPI M777 was connected to the negative input of a Tektronix AM 502 differential preamplifier. This, in series with an AM 501 operational amplifier (fixed gain of 10; ± 40 V output swing) constituted the voltage clamp amplifier. The gain of the AM 502 was usually set in the range 100–300, with a 3 db point at 10 or less frequently 3 kHz. Command signals were fed to the positive input of the AM 502, save for the holding potential command which was set using the 'DC offset' feature of the AM 502. In practice, the DC offset was positioned so that, with the clamp output disconnected, the overload light of the AM 502 did not glow even when the over-all gain was set to 10–20000. This meant that the cell was initially clamped to its resting potential.

The best performance of this clamp system was obtained when interelectrode coupling was minimized by careful shielding. Usually the voltage electrode was silver painted to within 0·5 mm of its tip, the distal paint layer being insulated with 'Q-dope'. The paint shield was then connected to the driven shield of the WPI headstage. A simple aluminium foil shield extended over the current electrode holder and that part of the current electrode close to unpainted portions of the voltage electrode. This foil shield was grounded. In some cases the current electrode was painted and grounded instead. This gave less noise under voltage clamp, but the extra capacity to ground often compromised the 'zap' circuit.

The clamp current was measured using a virtual ground circuit connected to a second AgCl pellet bath electrode. The entire perfusion system had to be electrically shielded to avoid line interference on the current monitor. However, line interference on the micro-electrode inputs was negligible because of short path lengths and driven shields, and no Faraday cage was used. The apparatus rested on an air-suspension antivibration table (Kinetic Systems).

Data logging and analysis. Voltage clamp records were displayed on a Tektronix storage oscilloscope and on a Gould 2400 chart recorder (frequency response flat to -3 db at approximately 100 Hz; rise time for full-scale deflexion ~ 8 ms). Chart records or Polaroid oscilloscope photographs were measured using a ruler or a transparent graph paper overlay.

Experimental procedure and limitations

Impalement of the current-passing electrode was usually accomplished first. The health of the cell was checked by injecting small hyperpolarizing or depolarizing currents using the WPI bridge facility. A cell was considered worthwhile if its resting potential exceeded -35 mV, and it exhibited a sharp spike. However, quite often singly impaled cells had resting potentials of -40 to -55 mV, with spike amplitudes of up to 100 mV. Even with very fine electrodes and careful impalement resting potentials negative to -60 mV were never encountered. (Average values of $-54 \pm 2{\cdot}8$ and $-48 \pm 8{\cdot}8$ mV have previously been reported for frog neurones by Blackman, Ginsborg & Ray (1963) and Hunt & Nelson (1965).) Insertion of the second electrode almost invariably led to some deterioration in membrane potential, spike amplitude or input resistance. Frequently, however, some improvement in the recording ensued in the next few minutes, and on occasion doubly impaled cells appeared to have sustained no more damage than the healthiest of singly impaled cells. However, only very rarely were we able to record from doubly impaled cells for the lengthy periods that are possible with singly impaled cells (or that we would have liked). Two types of cell demise were encountered. In one case the cell became progressively leakier, a situation that could sometimes be corrected by re-adjustment of the electrodes. In the other, a sudden and catastrophic inward current, developing within a few seconds, and unheralded by signs of deterioration, occurred. The latter situation was often encountered when low resistance electrodes were used, and may arise from leakage of KCl into the cell. Unfortunately low resistance current electrodes are necessary when evoking large outward currents.

The minimum criterion for cell health before proceeding with the experiment was a resting

potential of −30 mV or better. This translated into a cell whose M-current amplitude on depolarizing from −60 mV to −30 mV equalled or exceeded the size of the instantaneous leakage jump (see Fig. 2).

The somatic voltage clamp used in these studies had several limitations. Firstly, it is sometimes tedious or difficult to ensure the well shielded low resistance electrodes that can achieve rapid accurate point clamping in these cells. In favourable cases voltage steps that are complete in less than 100 μs, and capacity transients that are over by 200 μs, can be achieved, even for membrane currents of 100 nA or more. However, in most cases such performance was neither achieved nor desired, since the relaxation times studied were longer than 5 ms.

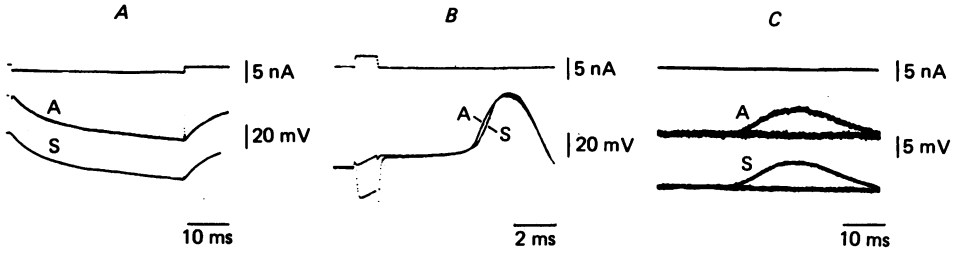

Fig. 1. Voltage records from a single neurone recorded through one electrode inserted into the soma (S) and another electrode inserted into the axon (A) about 150 μm from the soma. *A*, effect of hyperpolarizing current (upper beam) injected into the axon through a bridge circuit. *B*, superimposed action potentials triggered by a brief depolarizing current injection into the axon. (The downward deflexion of the voltage record obtained through the current-injecting electrode reflects bridge-imbalance.) *C*, spontaneous excitatory post-synaptic potential recorded in the soma and axon.

Three more insidious problems are poor space clamp, series resistance and ion accumulation. There is no doubt that the ganglion cell soma was essentially isopotential during clamp steps. Action potentials triggered by current injected through one electrode had identical time courses on both electrodes. Furthermore, insertion of a third, independent somatic electrode revealed the 'squareness' of the imposed membrane potentials. However, space clamp must fail at some point along the axon, which in all cases remained connected to the soma. In one unusual cell (Fig. 1) it was possible to visualize the axon over a distance of approximately 250 μm, and to separately impale both soma and axon, the total length of axon separating the recording site and the soma being about 150 μm. Spikes elicited by the axonal electrode preceded the somatic spike by about 0·2 ms, whereas spontaneous synaptic potentials occurred on somatic recording about 2 ms before the axonal counterpart. The electrotonic potential elicited in and recorded from the axon was indistinguishable from the somatically recorded electrotonic potential. This suggests that the first 150 μm of the bullfrog ganglion cell axon was also under good potential control. Undoubtedly, more distal, poorly clamped, axons contaminated the records. This was often seen as current notches for large depolarizing steps, or partially clamped 'anode break' responses following large hyperpolarizations from relatively depolarized holding potentials. Although amphibian axons exhibit more than one form of K^+ current (Dubois, 1981*b*), there appear to be no currents comparable to I_A, I_C or I_M; it is likely that the latter are mainly somatic, and therefore well clamped.

Possible series resistance was assessed by injecting a very large (20 nA) and very short (to prevent membrane breakdown) hyperpolarizing current pulse into a cell, and recording the resulting electrotonic potential on a fast sweep. The initial part of the charging curve should show an instantaneous component if there is appreciable series resistance. Unfortunately this part of the charging curve is obscured by interelectrode coupling artifacts, even when careful shielding and low resistance tips are used. By comparing the artifact recorded before and after destroying the cell membrane with a large voltage pulse, it was ascertained that any difference attributable to series resistance was less than 2 mV. Thus the series resistance present must be less than 100 kΩ. Since currents as large as 300 nA were sometimes encountered, potential error of up to 30 mV must be contemplated. However, the ion accumulation effects attendant on the passage of such large currents probably introduce even larger distortions and uncertainties than those due to possible

series resistance. These limitations apply primarily to large outward delayed rectifier and Ca^{2+}-activated currents. Their effects, and the means adopted for minimizing them, are referred to in the appropriate section of the Results. Their influence on the smaller ($\leqslant 5$ nA), slower M-currents was probably negligible.

RESULTS

(*A*) *The M-current*

The usual experimental protocol adopted for studying I_M is illustrated in Fig. 2*A*: the cell membrane potential was held under voltage clamp at a relatively depolarized level ($V_H = -30$ mV) and commanded to a more hyperpolarized level ($V = -60$ mV) for 0·5–1 s. I_M is a well developed steady outward current at -30 mV but is switched off in a time- and voltage-dependent manner during the hyperpolarizing command-pulse, producing the slow inward relaxation on the current trace. On repolarizing the cell I_M redevelops to produce a slow outward relaxation.

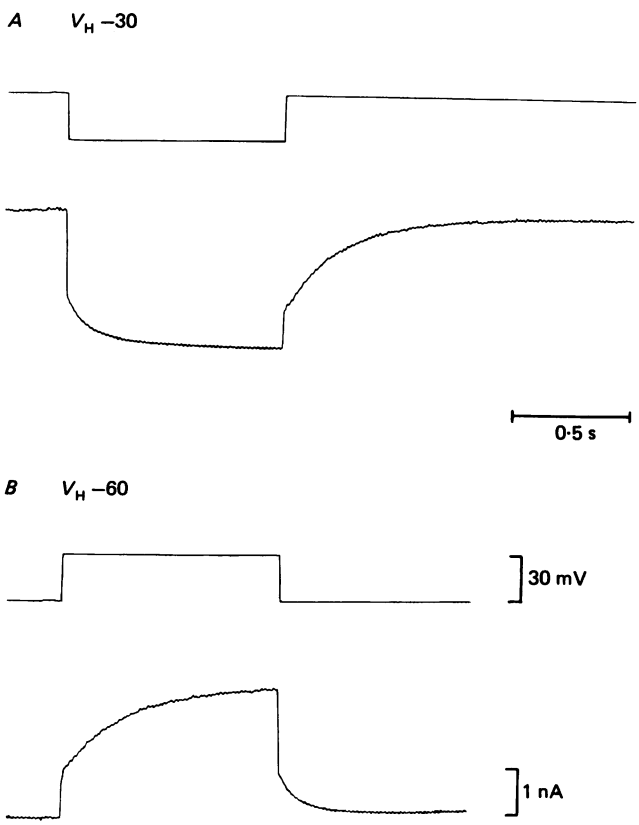

Fig. 2. Clamp-currents recorded from a bullfrog sympathetic neurone during (*A*) a 30 mV *hyper*polarizing voltage-command from a holding potential (V_H) of -30 mV and (*B*) a 30 mV *de*polarizing command from a holding potential of -60 mV. Upper trace, voltage; lower trace, current (outward current upwards). The slow inward and outward relaxations following the instantaneous current-steps reflect the deactivation and reactivation respectively of I_M (see text).

Comparable, but inverted, relaxations were obtained when the cell was held *continuously* at −60 mV and briefly *de*polarized to −30 mV (Fig. 2*B*). The amplitudes of the inward and outward relaxations and their kinetics were approximately the same using either holding potential, indicating that the kinetics were governed solely by the final potential and that there was no appreciable inactivation of I_M at −30 mV.

The lower holding potential was preferred for most experiments since (i) V_H was nearer to the resting potential obtained after impaling the cell with the two electrodes

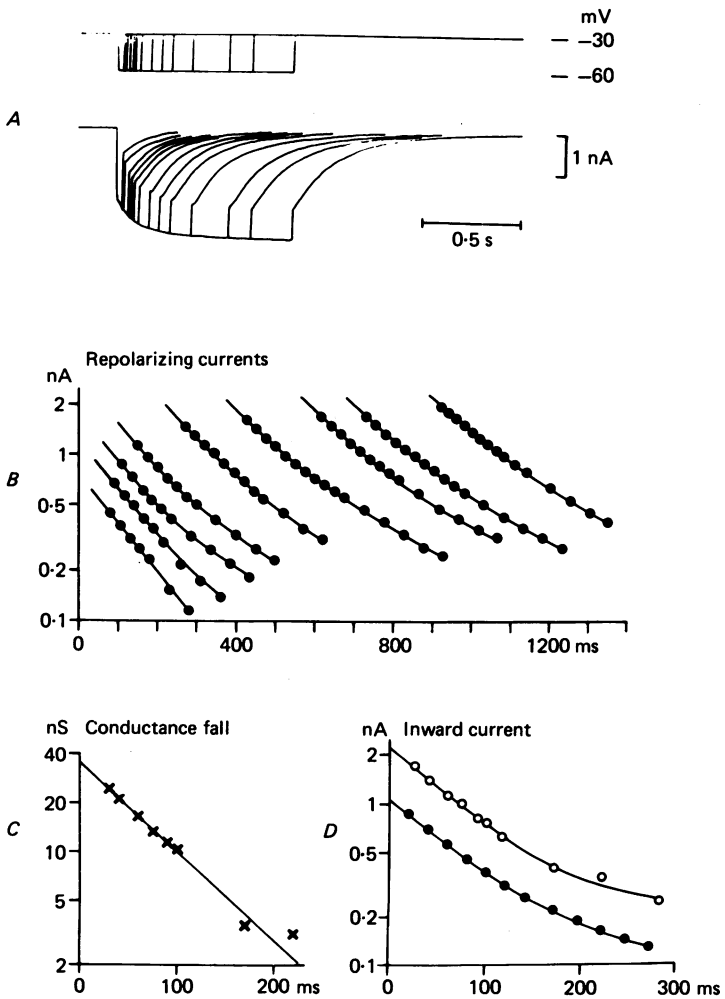

Fig. 3. *A*, superimposed tracings of current relaxations following a series of 30 mV hyperpolarizing step-commands from a holding potential (V_H) of −30 mV, similar to that illustrated in Fig. 2*A* but varying in duration between 30 and 890 ms. *B*, semi-logarithmic plots to show the time course of the slow outward (repolarizing) current-tails. *C*, time course of the fall in conductance accompanying the inward current relaxation during the hyperpolarizing voltage-step, measured from the amplitudes of the instantaneous current-steps generated on repolarizing to −30 mV (see text). *D*, time course of the recorded inward current during the longest (890 ms) hyperpolarizing command (●) and of the envelope of repolarizing current-tail amplitudes shown in *B* (○).

(usually between −35 and −45 mV, see Methods), so that a smaller holding current was necessary; (ii) the large outward currents appearing at membrane potentials above −25 mV were somewhat inactivated on holding at −30 mV (see below); and (iii) the presence of a standing M-current was useful in assessing the effects of ionic changes or pharmacological agents (see Brown, Adams & Constanti, 1981).

Conductance changes

The instantaneous current–voltage curve is approximately linear between −30 and −60 mV (see Fig. 5 below). Hence, comparison of the instantaneous current-steps (I_{in}) at the beginning and end of the hyperpolarizing command measures the change in membrane chord conductances G_{ch}. Thus, in Fig. 2*A* the initial value for I_{in} for a 30 mV jump was 1·8 nA, so G_{ch} prevailing at the holding potential was 60 nS. The value of I_{in} on repolarizing was 0·75 nA, so G_{ch} had fallen to 25 nS after 890 ms at −60 mV. G_{ch} remained at 25 nS on holding for some time at −60 mV, then increased to 58 nS after an 890 ms depolarizing command to −30 mV (Fig. 2*B*). Thus, the voltage-sensitive conductance affected by these 30 mV voltage jumps appears to fall to a steady-state level after 890 ms hyperpolarization at −60 mV and to be nearly completely re-established after 890 ms depolarization to −30 mV.

The *time-course* of the fall in conductance was examined more closely by varying the duration of the hyperpolarizing pulse between 30 and 890 ms (Fig. 3*A*) and measuring the amplitude of the instantaneous repolarizing current-step at each time t ($= I_{in}(60)_t$) and at 890 ms ($= I_{in}(60)_{890}$). Assuming a steady-state after 890 ms, the residual voltage-sensitive conductance

$$G_{ch}(60)_t - G_{ch}(60)_{890} = (I_{in}(60)_t - I_{in}(60)_{890}/(V - V_H))$$

showed an approximately exponential decline with a time-constant $\tau_G(60)$ of about 78 ms (Fig. 3*C*) and extrapolating to 35 nS at zero-time, in agreement with the estimate of the total voltage-sensitive conductance deduced from Fig. 2*A*. In five tests of this type, using hyperpolarizing pulses of up to 2 s duration, the mean value for $\tau_G(60)$ (±S.E.M.) was 90±4·6 ms. In a comparable series of tests using a 30 mV depolarizing voltage jump from a holding potential of −60 mV, the chord conductance showed an exponential increase to a steady-state with a mean time constant τ_G (30) of 185±14·7 ms ($n = 5$), about twice as long as the decay time constant.

Time course of the slow current-relaxations

The inward current-relaxation followed the time-course of the fall in conductance quite well for the first 100–150 ms of hyperpolarization (● in Fig. 3*D*), but showed appreciable deviation from a simple exponential at later times. This was a variable but frequent phenomenon, the response illustrated being fairly representative in this respect. It was not due to current drift since the time course of the recorded inward current was reproduced by that of the envelope of repolarizing outward currents (○ in Fig. 3*D*: cf. Noble & Tsien, 1968). Further, the outward currents themselves showed comparable slow 'tails' after long hyperpolarizing commands (Fig. 2*B*). Since the measurement of small residual conductances after prolonged hyperpolarization was of limited accuracy, it is not entirely clear whether or not there was a corresponding slow 'tail' to the decline in conductance: if so, this was very small.

Slow inward tails. Slow 'tails' have been described for outward K^+ currents in cardiac muscle (Brown, Clark & Noble, 1976; Di Francesco, Noma & Trautwein, 1979). One form of current-tail can arise from extracellular K^+ accumulation, with consequential shifts in E_K (Noble, 1976). This might apply to an inward current-tail if there were a steady accumulation of K^+ outside the cells at the holding potential which was relieved by hyperpolarization. However, two lines of evidence suggest this to be rather unlikely. Firstly, slow current tails were also detected in 25 mM-K^+

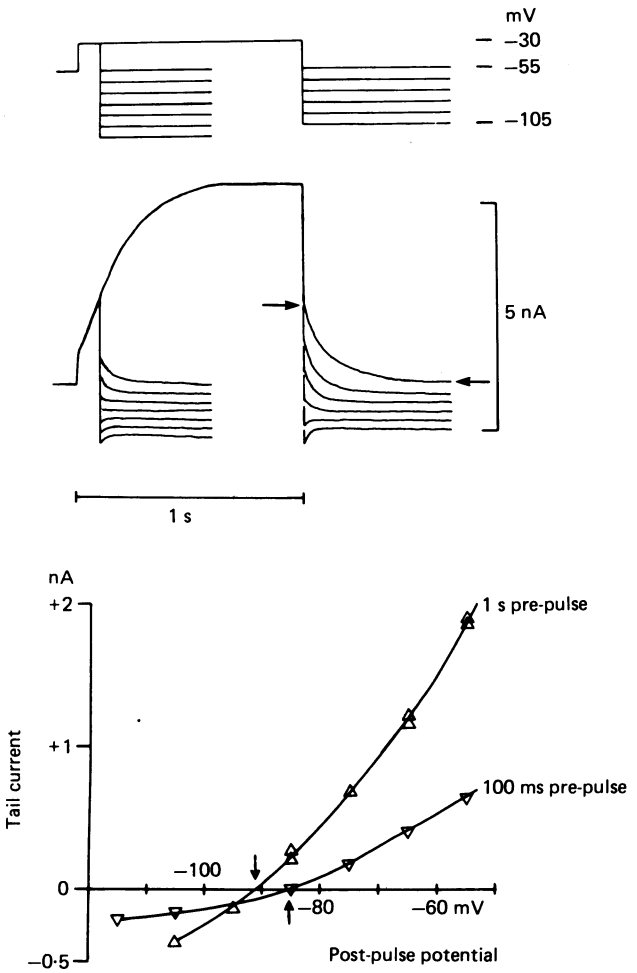

Fig. 4. Apparent reversal potential for I_M. The upper part of the Figure shows superimposed tracings of currents elicited by 100 ms and 1 s depolarizing commands to −30 mV from a holding potential of −55 mV, followed by repolarizing steps from −55 to −115 mV in 10 mV divisions. Upper record, voltage commands (schematic): lower record, currents. The graphs below show the initial amplitudes of the tail-currents (an example of how tail amplitude was estimated is given by the arrows delineating the −55 mV, 1 s tail in the upper records) plotted against post-pulse potential. A single series of measurements after a 100 ms depolarizing pulse was bracketed between two series of measurements after a 1 s pulse. Note that the reversal potential (arrowed) after full I_M activation (1 s pulses, −92 mV) is more negative than that (−85 mV) after the 100 ms pulse.

solution (the current-relaxation being *outward* at −60 mV under these conditions, see Fig. 6), in which changes in extracellular [K^+] are less likely. Secondly, where cells were held continuously at −60 mV and commanded to −30 mV for brief (100 ms) and long (1 s) periods, the reversal potential for the repolarizing tail currents tended to be *more* negative after a long pulse (by some 5–10 mV) than after a short pulse (Fig. 4). This is contrary to expectation were the generation of I_M to be associated with significant extracellular K^+ accumulation. (The converse experiment, of holding the cell at −30 mV and measuring the reversal potential for I_M after long and short hyperpolarizing commands, was impracticable because I_M declined too rapidly at hyperpolarized potentials.)

Slow inward current. An alternative explanation is that hyperpolarization can activate an additional, and quite separate, slow inward current. Appropriate, very slow, inward currents were frequently noted on hyperpolarizing the cell to −90 mV or more (see, for example, Fig. 12). At such voltages this current could easily be distinguished from the M-current since the I_M relaxation then becomes quite fast ($\tau_M \leqslant 10$ ms at −90 mV, see Fig. 8) and is usually inverted to an outward current. The slow inward current increased in amplitude with increasing hyperpolarizing commands at least to −140 mV. Though simple extrapolation suggests that it would be very small at −60 mV, it might be sufficient to confer a small but variable slow tail to the apparent I_M relaxation. Since the reversal potential for the slow inward current is clearly more positive than that for I_M (see below), its presence might also explain the small shift in the apparent reversal potential of the outward current with increasing depolarizing command duration: one might suppose that a long command pulse inactivated the slow inward current, so yielding a 'pure' I_M reversal potential, whereas a contribution of the slow inward current to the reversal potential persisted after a short depolarizing command.

Slow inward currents, activated by hyperpolarization and accompanied by an *increase* in conductance, have recently been described in rabbit sino-atrial nodal tissue (Noma & Irisawa, 1976; Yanagihara & Irisawa, 1980; Brown & Di Francesco, 1980) and in cat spinal motoneurones (Barrett, Barrett & Crill, 1980). The slow current in frog sympathetic neurones is somewhat comparable to these currents in the sense that it increased in amplitude with hyperpolarization, although we have not yet established whether it is associated with an increased conductance. A similar current is present in hippocampal neurones (Adams & Halliwell, 1982).

Isolation of the I_M relaxation from possible slow-current contamination by any form of 'curve-peeling' (cf. Brown *et al.* 1976) was impracticable in view of the variability and low amplitude of the tail, and we have insufficient information about the slow current to make any theoretical allowances. Instead, in subsequent kinetic experiments, time-analysis of the I_M relaxations was limited to the first 100–150 ms (see Di Francesco *et al.* 1979). In the sample of neurones used for conductance time course measurements, this method yielded average values for the time-constants for the inward current relaxation at −60 mV from a holding potential of −30 mV ($\tau_M(60)$) of 113 ± 15 ms, and for the outward relaxation at −30 mV from a holding potential of −60 mV ($\tau_M(30)$) of 206 ± 19·5 ms. These exceed the mean values of τ_G (the time constant for the conductance decline) by no more than 10–20 %. Since the conductance measurements are of limited accuracy and might themselves be distorted

by any small late conductance increase underlying the slow inward current-tail, these estimates of the initial current relaxations may be regarded as a reasonable measure of the time course of the conductance change underlying I_M.

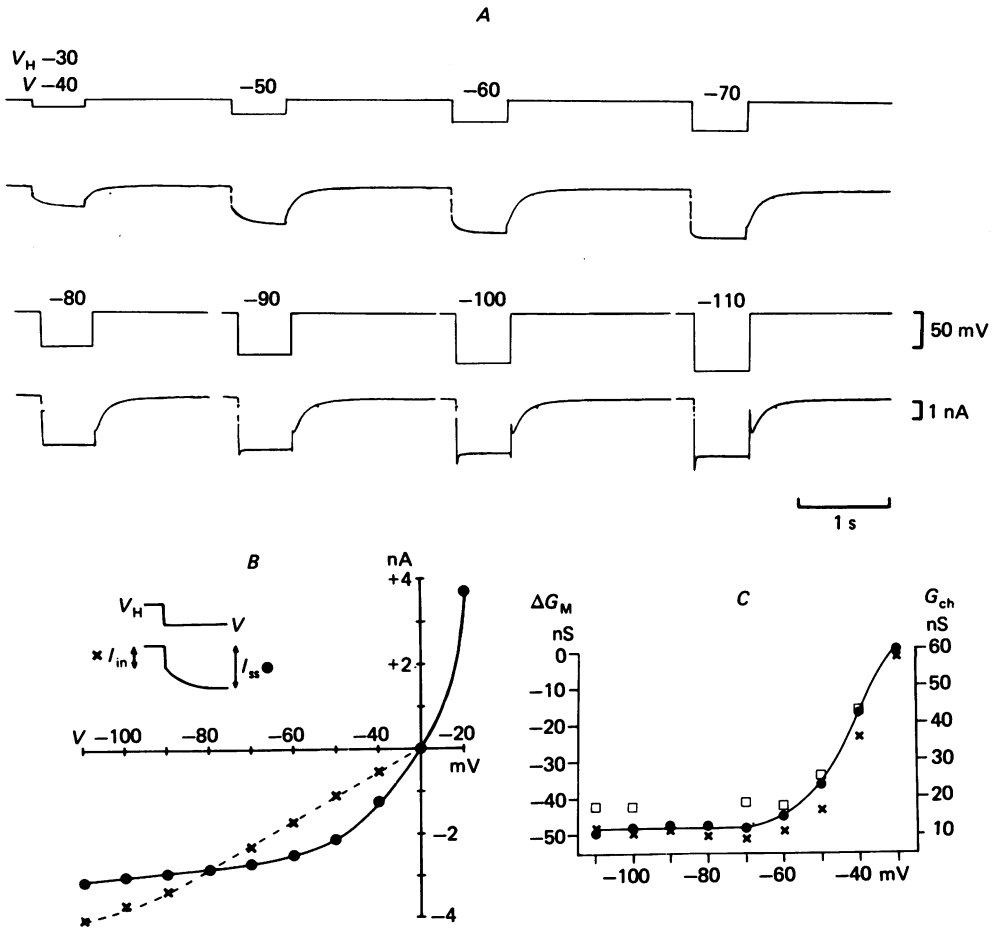

Fig. 5. Voltage dependence of I_M. *A*, clamp-currents recorded during a series of increasing hyperpolarizing command-steps from a holding potential of −30 mV (cf. Fig. 3*A*). *B*, instantaneous (×) and steady-state (●) current–voltage curves constructed from the records in *A* (plus a 10 mV depolarizing step, not shown). The 'instantaneous' currents (I_{in}) were the amplitudes of the initial inward current-steps at the onset of hyperpolarization; the steady-state current (I_{ss}) is the current level at the end of the voltage-command (holding current at −30 mV subtracted). *C*, change in M-conductance (ΔG_M) during each hyperpolarizing command calculated from the amplitudes of the slow current relaxations during the command-pulse (●) and the repolarizing tail-current (□). The crosses show the change in chord conductances (G_{ch}) calculated from the decline in amplitude of the instantaneous current-step between the onset and end of each hyperpolarizing command (cf. Fig. 3*D*).

Reversal potential for I_M

With hyperpolarizing commands increasing in 10 mV steps from a holding potential of −30 mV, the inward I_M relaxation first increased in amplitude, then diminished and finally reversed to a quite rapid outward relaxation (Fig. 5). This

reversal is depicted graphically by the intersection of the instantaneous and steady-state current–voltage curves in Fig. 5*B*. In a sample of twenty-three cells held at −30 mV in 2·5 mM-K^+ solution, the mean reversal potential for I_M(= V_M) was −85·8±2·1 (S.E.M.) mV. Varying the holding potential between −30 and −50 mV did not alter V_M for the inward relaxation by more than 5 mV (three cells).

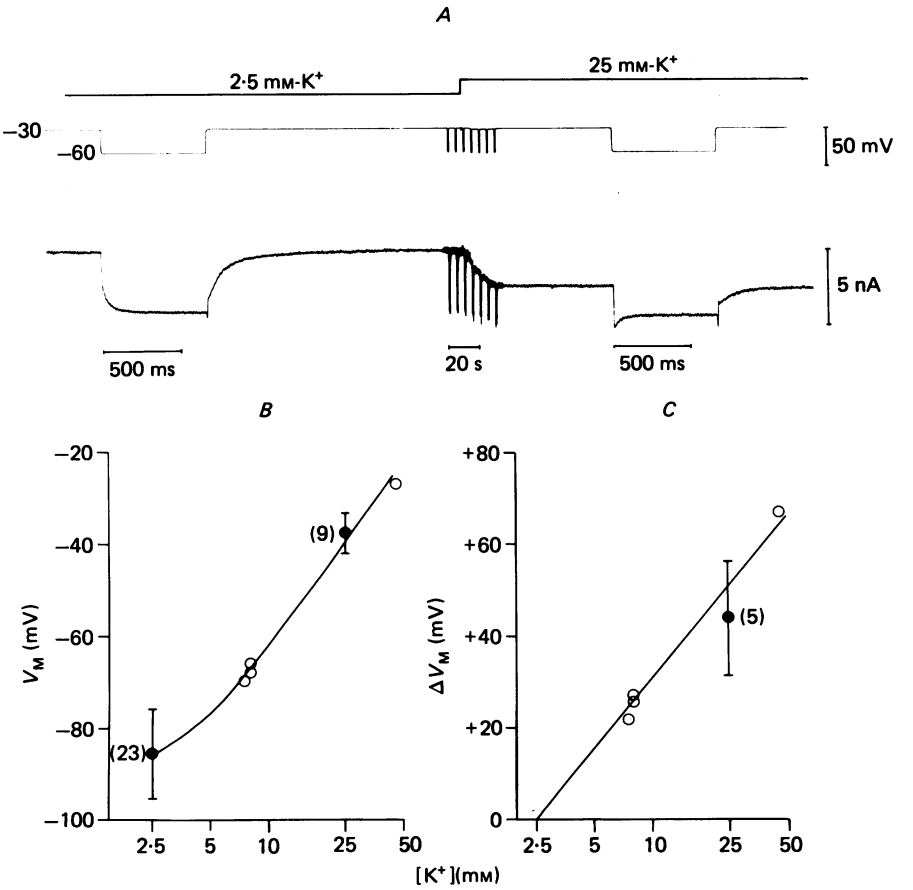

Fig. 6. *A*, effect of raising $[K^+]_{out}$ from 2·5 to 25 mM on the current relaxations evoked by 30 mV hyperpolarizing commands from a holding potential of −30 mV. Note that the slow current relaxation during hyperpolarization reverses from inward in 2·5 mM-K^+ to outward in 25 mM-K^+. *B*, reversal potentials (V_M) for I_M plotted against $[K^+]_{out}$. Filled symbols (●): mean (*n* in brackets; bars show standard deviations); open symbols: single cell measurements. Reversal potentials were measured from the intersection of instantaneous and steady-state current–voltage curves. (Curve drawn by eye.) *C*, shifts in V_M on raising $[K^+]_{out}$ from 2·5 to 7·5, 8, 25 or 47·5 mM, measured in separate cells as described in the text.

Concordant values of −72, −86, −91 and −95 mV (in four cells) were obtained for the reversal potential of the current-tails following a 1 s depolarizing pulse to −30mV from a more negative holding potential, determined in the manner illustrated in Fig. 4, indicating that the reversal potentials for a transient or steady-state outward current at −30 mV were the same.

Effect of K^+ on V_M. Fig. 6 illustrates the effect of raising external K^+ ten times

(from 2·5 to 25 mM) on the I_M relaxations produced by jumping from −30 to −60 mV. The normal inward relaxation at −60 mV is inverted to an *outward* relaxation, i.e. the initial M-current (prior to the relaxation) is now *inward* at −60 mV. Since the repolarizing current-tail remains outward, this implies that the reversal potential for I_M now lies somewhere between −30 and −60 mV. If the amplitude of the inward I_M relaxation on hyperpolarizing the cell to command potential V is designated $I_M(V)$ and the amplitude of the outward relaxation on repolarizing from V to the holding potential V_H is designated $I_M(V_H)$, then assuming a linear I–V relationship the ratio of these currents (r) is given by

$$r = \frac{I_M(V)}{I_M(V_H)} = \frac{(V_M - V)}{(V_H - V_M)},$$

whence the reversal potential V_M is

$$V_M = \frac{(rV_H + V)}{1 + r}.$$

This calculation, applied to the sample records in Fig. 6, yielded values of −86 and −48 mV for V_M in 2·5 and 25 mM-K^+_{out} respectively. (The former value agreed with that obtained from the intersection of instantaneous and steady-state current–voltage curves in 2·5 mM-K^+ in this experiment.) In a sample of nine cells, the mean value of V_M in 25 mM-K^+_{out} calculated in this manner was −37·8 ± S.E.M. 1·54 mV.

The addition of 22·5 mM-K^+ in this (and other) experiments produced a net inward increase in the steady holding current at −30 mV. This is to be expected from the reduced driving force for the steady outward M-current; indeed, in the example illustrated in Fig. 6, the amplitude of this inward current approximately equals the amount by which the repolarizing slow current is reduced. Likewise, the kinetics of the inward and outward relaxations are not materially altered, and the instantaneous current step is only slightly increased in 25 mM-K^+. Thus, K^+ ions do not greatly modify I_M other than by altering its driving force.

Fig. 6*B* shows how V_M varied at different K^+ concentrations. The mean slope corresponded to 49 mV depolarization/10-fold elevation of $[K^+]_{out}$ the slope above 7·5 mM-K^+_{out} was about 58 mV. Fig. 6*C* shows the mean *shift* in V_M on raising $[K^+]_{out}$ from 2·5 to 7·5, 8, 25 or 47 mM (taken from a more restricted sample of cells in which measurements at two different values of $[K^+]_{out}$ were made): the mean slope was 52 mV/10-fold elevation. These experiments indicate that I_M is substantially, if not exclusively, a K^+ current.

Rb^+ and Cs^+. These ions were tested in five cells. Addition of 5 mM-Rb^+ to 2·5 mM-K^+ raised V_M by 18 and 20 mV (two cells); addition of 5 mM-Cs^+ raised V_M by $\leqslant 3$ mV (four cells). This suggests a ratio of $1:0{\cdot}5:< 0{\cdot}1$ for $P_K:P_{Rb}:P_{Cs}$ in carrying I_M. However, whereas neither K^+ nor Rb^+ changed the apparent conductance G_M (measured as $I_M(30)/(V_H - V_M)$), 5 mM-Cs^+ reduced G_M by up to 30 %, implying that Cs^+ had an additional partial-blocking action.

Chloride. Substituting NaCl with Na isethionate (i.e. reducing external (Cl^-) from 142 to 27 mM) did not clearly modify V_M or the kinetics of the I_M relaxation (two cells).

Isethionate substitution produced a 6 mV junction potential change at the virtual ground electrode, such that extra inward current was injected to depolarize the cell by 6 mV. A change in V_H of this magnitude was readily apparent from the current records from the fact that V_H now exceeded the threshold for the large outward currents, which (though inactivated on holding at −24 mV) were reactivated on repolarization after the hyperpolarizing command, producing a very characteristic overshoot in the repolarizing current-trace. This allowed an approximate correction for the junction-potential shift during the experiment itself, by adjusting the nominal clamp-potential to remove the overshoot. Elevation of $[K^+]_{out}$ to 25 mM produced a smaller junction potential change ($\leqslant$ 2 mV) which was not corrected but which might account (for example) for the apparent increase in I_{in} (30) in Fig. 6, since the voltage sensitivity of the conductance is near its steepest around −30 mV (see Fig. 8 below).

I_M activation

The total amplitudes of the I_M relaxation during and after each of the series of hyperpolarizing commands shown in Fig. 5 provide a measure of the deactivation and reactivation of I_M. The underlying conductance change is then yielded by dividing the relaxation amplitude by the driving force. Thus, for deactivation at command potential V, $-\Delta G_M(V) = -\Delta I_M(V)/(V - V_M)$, where V_M is the reversal potential; and, for activation on returning to V_H, $+\Delta G_M(V_H) = +\Delta I_M(V_H)/(V_H - V_M)$. Assuming no change in V_M during the command, and no strong rectification, these two measures of ΔG_M should be equivalent. As shown in Fig. 5*C*, this was approximately so, at least within the range (−30 to −70 mV) where both inward and outward current relaxations could be measured with reasonable accuracy.

The results of such measurements suggested that G_M is fully deactivated at membrane potentials of −70 mV or greater. However, the behaviour of I_M at more negative potentials than −70 mV could not be followed very clearly using the experimental protocol illustrated in Fig. 5, for two reasons: firstly, the off currents were very small between −70 and −100 mV, since this straddles V_M; and secondly the initial part of the repolarizing current was obscured by a fast transient outward current, I_A (see below and Fig. 5*A*). To explore this region of membrane potential, hyperpolarizing jumps of the type illustrated in Fig. 5 were made in 25 mM-K^+ solution: the deactivated current is then outwards at all potentials more negative than −40 mV (see Fig. 6) and can be measured fairly easily down to −100 mV. Experiments of this type confirmed that I_M is fully deactivated beyond −70 mV.

Activation of I_M by depolarizing commands to membrane potentials more positive than −30 mV is accompanied by activation of large outward currents. Notwithstanding, the activation curve for I_M could be pursued over a limited range (up to −10 mV and, occasionally, to 0 mV) by examining the repolarizing tail-currents (Fig. 7). I_M contributes a clear slow component to the tail-currents, which is abolished by pharmacological agents suppressing I_M (see fig. 4 in Brown & Adams, 1980). Extrapolation of this slow component (Fig. 7*B*) suggests that I_M is fully activated by −10 mV.

Fig. 8*A* (●) summarizes estimates of G_M activation drawn from twenty-two experiments of the type illustrated in Fig. 5, using a holding potential of −30 mV and command potentials ranging from −100 to −10 mV. ΔG_M was measured from the initial amplitudes of the extrapolated repolarizing tail-currents at −30 mV, and the total M-conductance, G_M, calculated by subtracting each value of ΔG_M from that

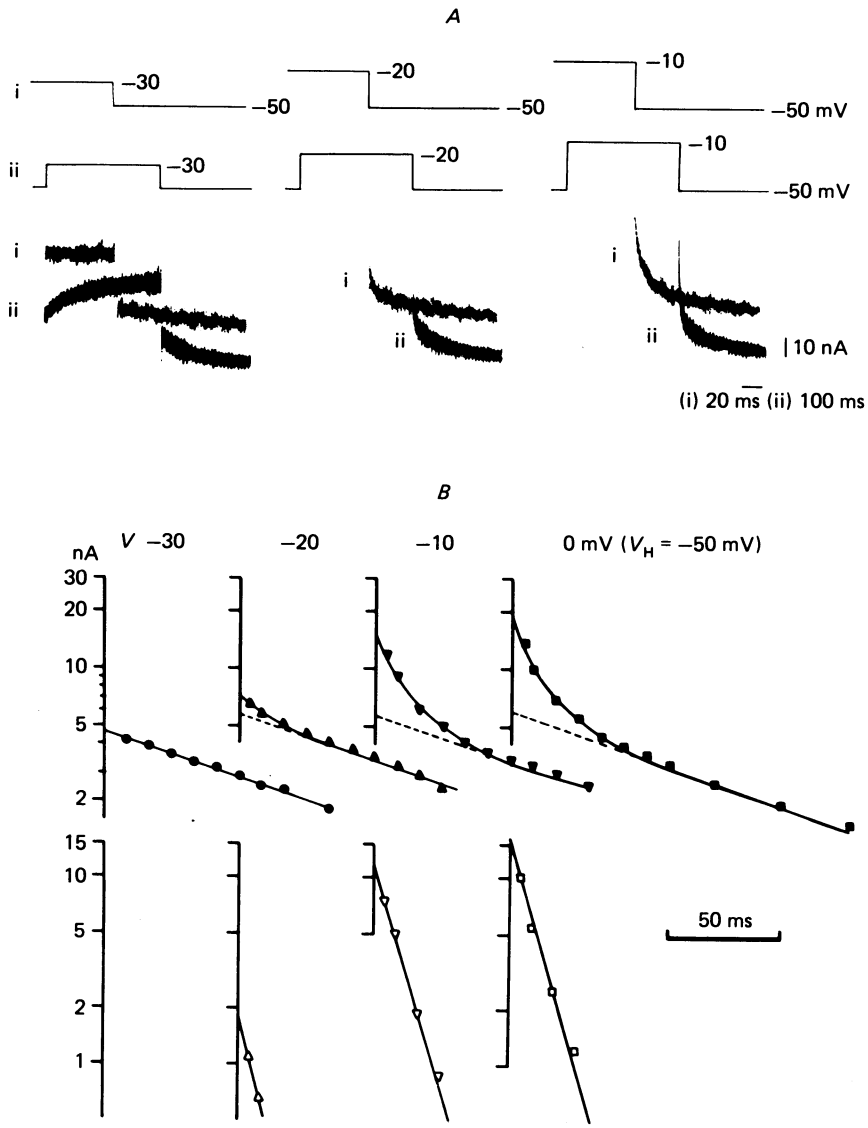

Fig. 7. Separation of M-current tails (I_M) and delayed rectifier current-tails (I_K) following 600 ms depolarizing commands from a holding potential of −50 mV. The records in *A* show repolarizing tail-currents from command potentials of −30, −20 and −10 mV recorded at two different sweep-speeds (i and ii). Except for the first pulse (to −30 mV), which activated only I_M, the outward currents are off-scale. The plots in *B* show semi-logarithmic time-plots of the total repolarizing tail-currents (upper graphs) and the fast I_K tail derived by subtracting the extrapolated slow I_M tail from the total tail-current (lower graphs). The apparent time-constant for the fast (I_K) tail was about 10 ms, that for the slow (I_M) tail about 120 ms. Note that I_M appears to maximize between −20 and 0 mV, and that the threshold for I_K is about −20 mV.

measured after repolarizing from −70 mV. Thus, G_M at −30 mV ($G_M(30)$) is taken as ΔG_M on repolarizing to −30 mV from −70 mV (= $\Delta G_M(70)$); G_M at −40 mV ($G_M(40)$) is then given by $\Delta G_M(70)$ *minus* $\Delta G_M(40)$; and so on.

The results suggest that G_M increases sigmoidally with voltage, with a half maximal value at −35 mV, and extrapolates to a maximum value of 84 ± 14 nS (mean ± S.E.M.) per cell. A plot of ln $G_M/(\bar{G}_M - G_M)$ against membrane potential yielded a slope of ~ 10 mV/*e*-fold increase in G_M (inset, Fig. 8*A*).

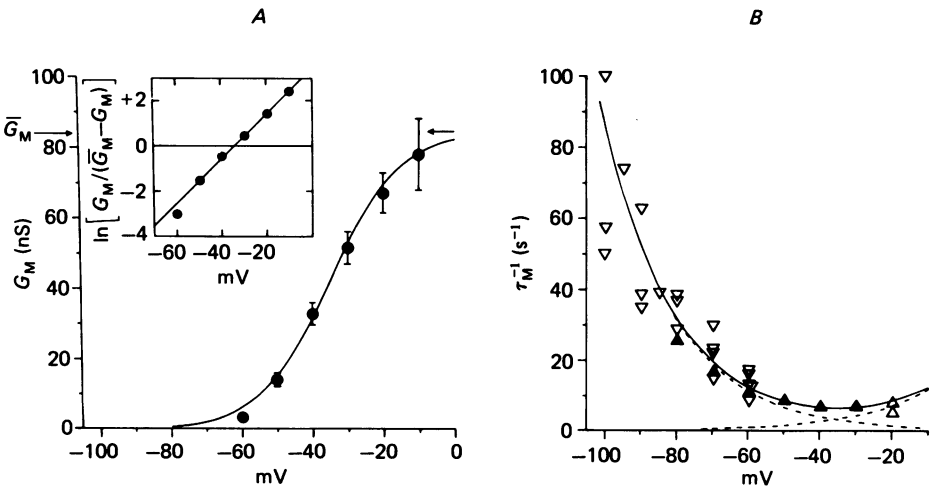

Fig. 8. Mean voltage dependence of (*A*) steady-state M-conductance G_M (nS) and (*B*) reciprocal time-constant for I_M relaxations, τ_M^{-1} (s^{-1}). Points in *A* were derived from twenty-two experiments of the type illustrated in Fig. 5 ($n = 6$ at −10 mV, 19 at −20 mV, 22 otherwise; bars = S.E. of mean where this exceeds point size). *Inset*: plot of ln $[(G_M/(\bar{G}_M - G_M))]$ against membrane potential ($\bar{G}_M$ = 84 nS); the line has a slope of 10 mV per ln unit. Different symbols in *B* refer to measurements in 2·5 mM-K^+ (△, ▲; nineteen experiments) and 8 or 25 mM-K^+ (▽; two experiments in 8 mM-K^+, three experiments in 25 mM-K^+) respectively. Open symbols: single measurements; filled symbols, means (n = 13–19; S.E.M. less than point size). Curves in *A* and *B* are drawn according to eqns. (3), (4) and (5). Arrows in *A* show extrapolated maximum conductance $\bar{G}_M$.

The position and amplitude of this activation curve was independent of holding potential within the range −50 to −25 mV, i.e. over the steepest part of the activation curve. Thus, in the cell illustrated in Fig. 9, current–voltage relations of the type illustrated in Fig. 5, extending between −100 and −10 mV, were constructed from three different holding potentials, −50, −40 and twice at −30 mV. The amplitudes of the slow component of the repolarizing current-tails $I_M(V_H)$ showed the same qualitative relationship to command-potential at each holding potential (Fig. 9*A*). The apparent reversal potentials (V_M) were −87, −87 and −92 mV at −30, −40 and −50 mV respectively; after allowing for the change in driving force ($V_H - V_M$), the conductance–voltage relationships at the three holding potentials were well aligned, and comparable to those shown in Fig. 8. Thus, there appears to be neither inactivation of I_M nor significant steady-state rectification (cf. Fig. 9 in Noble & Tsien, 1968) within the activation range for G_M.

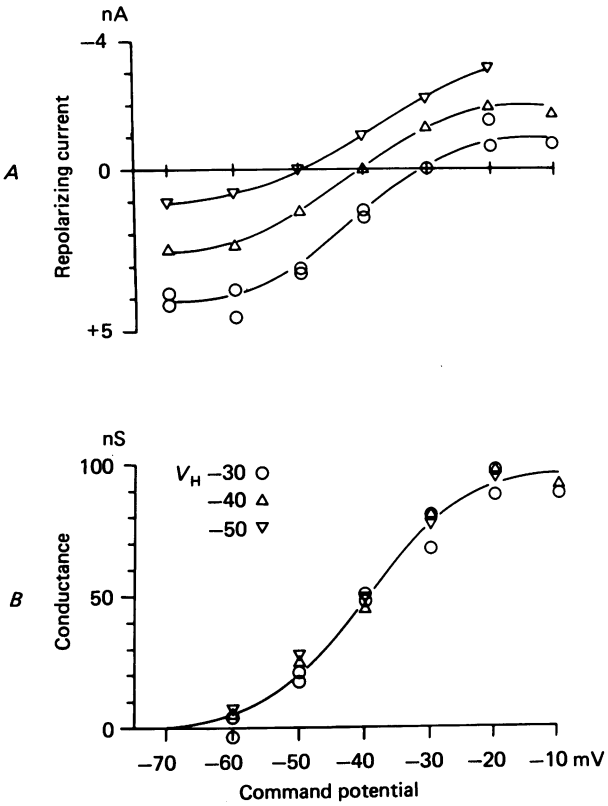

Fig. 9. *A*, amplitudes of the repolarizing I_M tail-current following 700 ms stepped-commands from three different holding potentials (○, −30 mV; △, −40 mV and ▽, −50 mV) recorded in a single neurone. I_M tails after depolarizing commands to −20 and −10 mV were isolated from I_K in the manner shown in Fig. 7. *B*, apparent conductance G_M obtained by dividing the currents in *A* by the driving force (holding potential *less* reversal potential for I_M), and summed to give the cumulative conductance from −70 mV. Note that the amplitude of G_M is unaffected by the change in holding potential.

Kinetics of I_M

It is apparent from Fig. 3 that the inward current at −60 mV was faster than the repolarizing outward currents measured at −30 mV. This difference is a function of the final membrane potential rather than the direction of the current, since both inward and outward currents followed the same kinetics when recorded at the same command potential (Fig. 10).

In the records shown in Fig. 5*A*, the inward I_M relaxation during a hyperpolarizing voltage-jump obviously accelerated as the command potential became more negative; the time constants (τ_M) were 150 ms at −40 mV command potential, 112 ms at −50 mV, 74 ms at −60 mV and about 44 ms at −70 mV. It was not possible to pursue these measurements to more hyperpolarized levels in normal Ringer solution, as the command potential then straddled V_K and the currents became too small. To obviate this difficulty, the K^+ concentration was raised to 25 mM and the time course of the *inverted* currents measured, as illustrated in Fig. 11. These experiments confirmed that τ_M continued to shorten down to some 10 ms or so at −100 mV. The

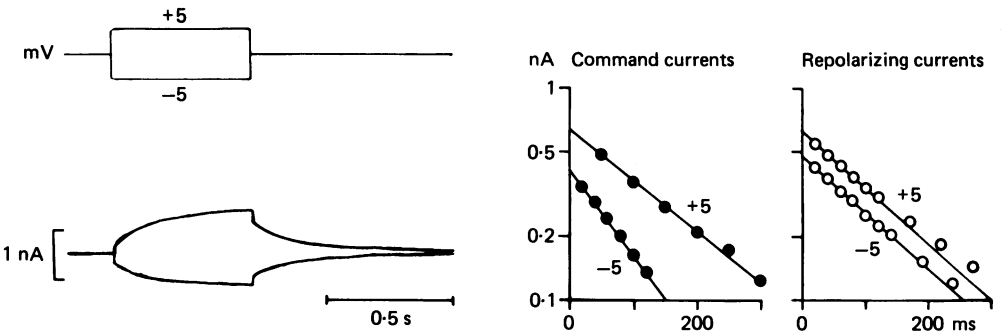

Fig. 10. Currents evoked by small (±5 mV) depolarizing and hyperpolarizing command-steps from a holding potential of −35 mV. Superimposed pen tracings of currents are shown on the left. The graphs on the right show semi-logarithmic plots of the time course of the slow current relaxations during the voltage command-steps (●, 'command currents') and the repolarizing tail-currents (○, 'repolarizing currents'). Note that the time courses of the command currents diverge whereas those of the tail-currents are similar.

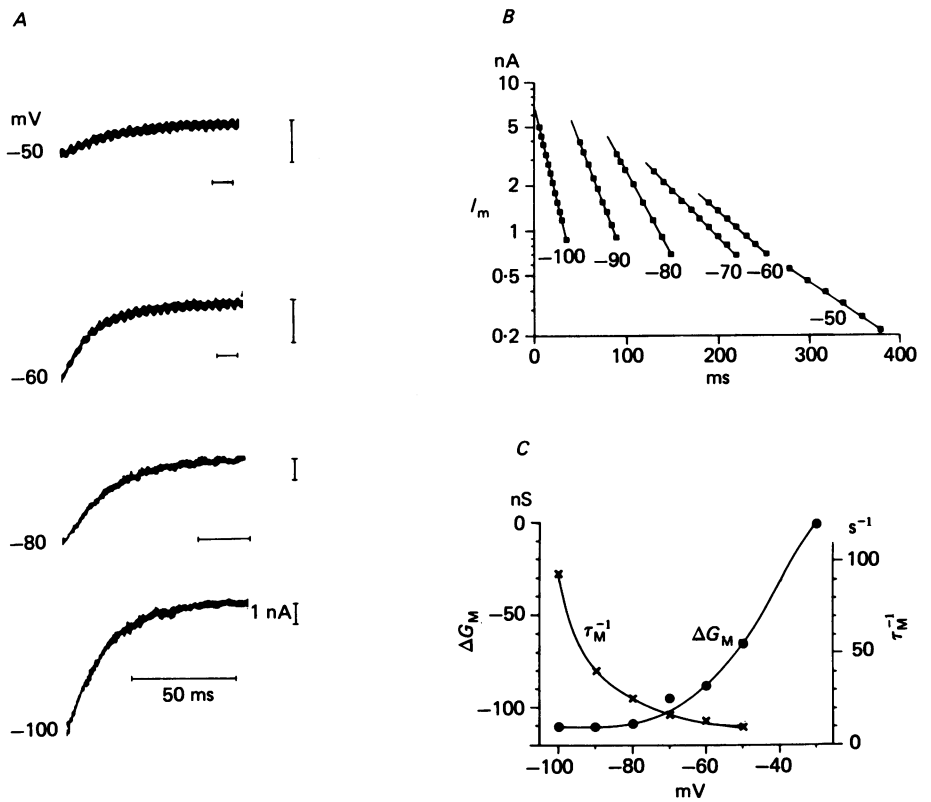

Fig. 11. M-currents recorded in 25 mM-K^+ solution. *A*, oscilloscope records of some inverted currents recorded following stepped commands to the membrane potentials indicated from a holding potential of −30 mV. Note the varying calibration scales. *B*, semi-logarithmic plots of the current time courses. *C*, fall in conductance (ΔG_M, ●) and reciprocal time constant (τ_M^{-1}, ×) deduced from the current relaxations plotted against command potential. G_M was calculated from the initial amplitudes of the slow relaxations divided by the command potential *less* the reversal potential (about −40 mV).

time-constants of the inverted currents in high $[K^+]$ agreed with those of the inward relaxations in normal Ringer at those command potentials (between -70 and -50 mV) where they could both be measured with reasonable accuracy, so raising $[K^+]_{out}$ did not itself materially alter the kinetics. In contrast to the closure relaxations, the outward relaxations observed on returning to the holding potential did not vary with the command potential attained in the preceding voltage-jump, as indicated in Fig. 5*A*.

Mean values for the rate constant for $I_M(=\tau_M^{-1})$ in 2·5 mM-K^+ (sixteen cells), 8 mM-K^+ (two cells), and 25 mM-K^+ (three cells), held at -30 mV, are summarized in Fig. 8*B*. The rate constant appears to attain a minimum value between -30 and -40 mV, mean values for τ_M at these two voltages being indistinguishable (158 ± 11 ms at -30 mV, 162 ± 12 ms at -40 mV, mean ± S.E.M.). Unfortunately, τ_M could not be estimated at more depolarized levels because of interference by the large outward currents.

Kinetic description of G_M and τ_M

The sigmoidal conductance–voltage relationship shown in Fig. 8 and the symmetrical exponential form of the on- and off-currents (Fig. 10) suggests that G_M follows a simplified form of Hodgkin–Huxley kinetics, in which the opening or closing of M channels are controlled by a *single* voltage-sensing particle (cf. Hodgkin & Huxley, 1952). Thus, we assume that the total conductance is the sum of the conductance of a number of identical channels, each of which has only two conductance states, open or shut, so that

$$G_M = \bar{G}_M y_M(\infty), \tag{1}$$

where $y_M(\infty)$ is the fraction of M channels in the open configuration at the steady-state and $\bar{G}_M$ is the maximal conductance where $y_M(\infty) = 1$. We also suppose that the probability of a channel being in the open configuration is governed by a Boltzmann distribution such that

$$y_M(\infty) = \left\{1 + \exp\frac{ze}{kT}(V_0 - V)\right\}^{-1} \tag{2}$$

(cf. Ehrenstein, Blumenthal, Latorre & Lecar, 1974), where z is the effective valency of the voltage-sensing particle, V is the membrane potential (inside negative) V_0 is the membrane potential where $y_M(\infty) = 0{\cdot}5$, and $e/kT(= F/RT) = 0{\cdot}04$. Combining eqns. (1) and (2):

$$G_M = \bar{G}_M\left\{1 + \exp\frac{ze}{kT}(V_0 - V)\right\}^{-1}. \tag{3}$$

The smooth curve in Fig. 8*A* shows a plot of eqn. (3) taking values of $\bar{G}_M = 84$ nS, $z = +2{\cdot}5$ and $V_0 = -35$ mV.

The voltage sensitivity of the time constant τ_M may then be expressed as:

$$\tau_M^{-1} = \alpha_M + \beta_M, \tag{4}$$

where α_M and β_M are opening and closing rate constants, varying with voltage as:

$$\alpha_M = \alpha_M(0)\exp\frac{+ze}{2kT}(V - V_0), \tag{5a}$$

and

$$\beta_M = \beta_M(0)\exp\frac{-ze}{2kT}(V - V_0), \tag{5b}$$

with $\alpha_M(0) = \beta_M(0) = 3{\cdot}3\ s^{-1}$ at $V = V_0$. Appropriate curves in Fig. 8*B* appear to describe the observed variation in τ_M^{-1} between -30 and -100 mV, suggesting that the expression for β_M at least is reasonable. The validity of the expression for α_M remains somewhat conjectural in the absence of firm data on τ_M at more depolarized levels.

I_M under current clamp

The time-dependent changes in I_M observed under voltage clamp following rapid membrane potential displacement are reflected by distinctive time-dependent rectifications in the membrane potential responses to current injection under 'current-clamp' conditions. Fig. 12 shows a sequence of current-clamp voltage trajectories (upper records) and matching voltage-clamp current responses (lower records) obtained in the same cell in normal and elevated K^+ solution. Thus, in 2·5 mM-K^+, a small current injection of $-1{\cdot}1$ nA for 600 ms, sufficient to drive the membrane potential from its resting value of -45 mV to a minimum value of -60 mV, results in a secondary depolarizing 'sag' to the voltage trajectory, corresponding to the inward I_M relaxation observed under voltage clamp at a command potential of -60 mV (upper left panel of Fig. 12). When the current injection is terminated, there is a rebound depolarization above the resting potential, corresponding to the redeveloping outward M-current. (In this record, the rebound depolarization is partly obscured by the spikes but its residuum is clear: it is *not* consequential to spike generation, since it could be seen in the absence of spikes.) As the injected current pulse was increased in amplitude to $-3{\cdot}1$ nA, so that the membrane potential was driven to the reversal potential for I_M (about -90 mV in this cell), the depolarizing sag to the voltage trajectory was eliminated (left-hand middle records of Fig. 12). Finally, with very large current injections a further, slower rectification is seen associated with the small second inward currents referred to earlier (lower left record). The initial I_M relaxation at very negative potentials is now outward, but is too rapid and small in 2·5 mM-K^+ to produce any very clear effect on the initial voltage trajectory. However, in elevated [K^+] this outward relaxation is much more pronounced at all membrane potentials negative to -40 mV, and is clearly manifest as a time-dependent *outward* rectification in the voltage trajectories.

There is also a good 'match' between the 'steady-state' rectification of the current–voltage curves (measured after 600 ms, Fig. 13) recorded under current and voltage clamp (except for a more pronounced anomalous rectification induced by the slow inward current at hyperpolarized levels in high K^+-solutions).

The time-dependent and steady-state rectification induced by I_M is considered further in the Discussion.

(B) Other K^+ currents

Three other K^+-currents were discerned in these neurones: two large outward currents readily activated from holding potentials between -60 and -30 mV (one conforming to a delayed rectifier current and one dependent on an inward Ca^{2+} current); and a transient outward current which was inactivated at membrane potentials more positive than -60 mV but which could be activated from more hyperpolarized levels. Since these currents appear analogous to currents previously described in invertebrate neurones, we have used the same insignia, I_K, I_C and I_A

respectively (see Thompson, 1977). Kinetic data on these currents in frog neurones is, as yet, less complete than that for I_M: the essentially qualitative description below is intended primarily to indicate how the currents differ from each other and from I_M. Such quantitative information as we present should be regarded as an approximation.

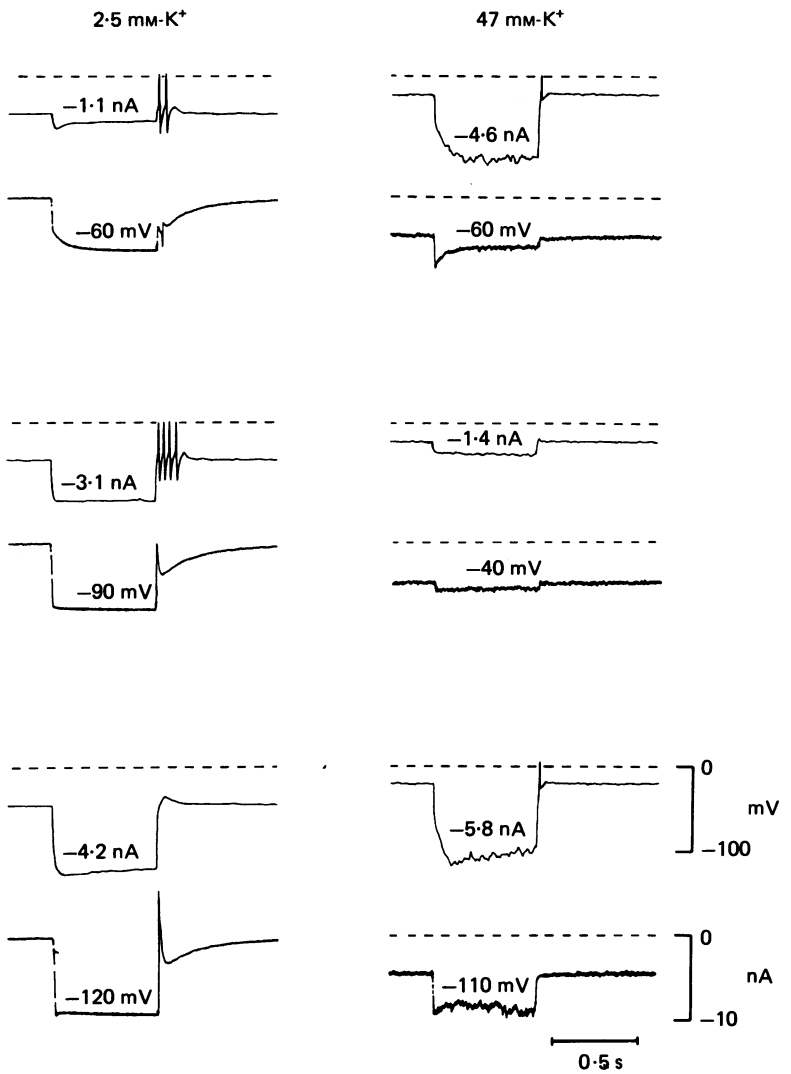

Fig. 12. Comparison of voltage-clamp and current-clamp observations in a single neurone recorded in 2·5 and 47 mM-K^+_{out}. Records show sample voltage-trajectories produced by 0·6 s hyperpolarizing current injections (upper records) and clamp-currents produced by hyperpolarizing voltage-commands (lower records). The command current and voltage pulses are omitted for simplicity, but their values are inserted on the records, as current injection (nA) or command potential (mV; V_H −30 mV under voltage clamp). Dashed lines show zero potential; resting potentials, −45 mV in 2·5 mM-K^+, −27 mV in 47 mM-K^+. The increased 'noise' on both voltage and current records in raised [K^+] probably results from K^+-induced transmitter release. (See text for further details.)

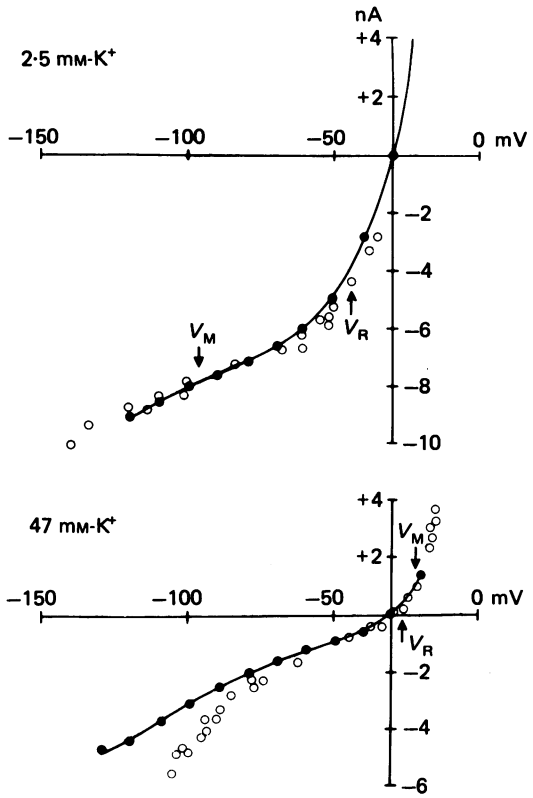

Fig. 13. Current–voltage curves constructed from the experiment illustrated in Fig. 12 for voltage-clamp (●) and current-clamp (○) data. Responses were measured after 600 ms. V_M = reversal potential for I_M; V_R = rest potential under current-clamp.

Delayed rectifier current (I_K)

In order to isolate I_K from other currents, cells were usually treated with tetrodotoxin (TTX, 0·5 μM) to depress Na^+ currents and bathed in a Ca-free solution containing 0·1–0·5 mM-Cd^{2+} to inhibit inward Ca^{2+} currents (Adams, 1980) and reduce the component of outward current attributable to I_C (see below). (The high concentrations of TTX required to suppress the fast inward current and/or spikes may have been an effect of trypsin: cf. Lee, Weeks, Kao, Akaike & Brown (1979).) A further difficulty was presented by the large size of the outward currents – up to 300 nA – generated at potentials positive to zero in normal Ringer solution. In addition to errors induced through any series resistance (see Methods), the repolarizing tail-currents showed a complex time course and very depolarized reversal potentials (usually positive to −50 mV) suggesting large and rapid shifts in perineuronal $[K^+]$ (cf. Frankenhaeuser & Hodgkin, 1956; Maugham, 1973; Dubois & Bergmann, 1975; Dubois, 1981*a*). This difficulty was reduced (though not eliminated) by raising $[K^+]_{out}$ to 25 or 47 mM.

Fig. 14 illustrates some outward currents generated under these experimental conditions. The currents clearly have the sigmoidal time course normally associated

with the delayed rectifier current (cf. Hodgkin & Huxley, 1952*b*). In contrast, the repolarizing tail-currents showed a simple exponential decay with time.

The conductance at the end of the 100 ms pulse was measured by dividing the current amplitude (either the end of the on-current after leak correction, or – more conveniently – the initial tail-current amplitude) by the driving force $V - V_K$ or

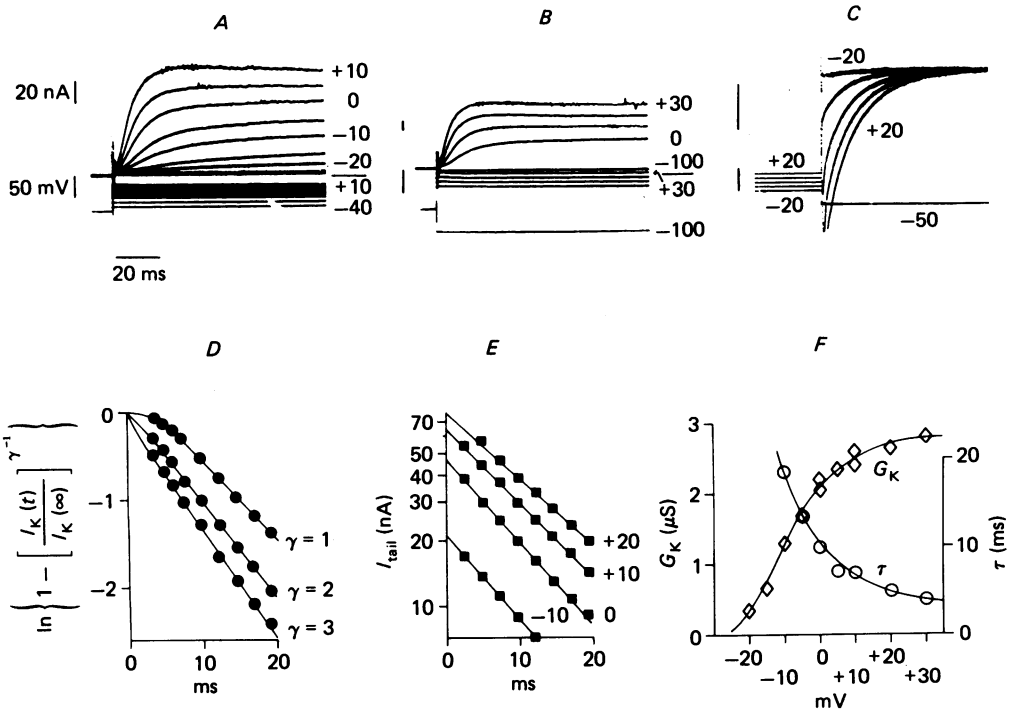

Fig. 14. Delayed rectifier currents (I_K) recorded in a solution containing 25 mM-K^+, 0 mM-Ca^{2+} and 0·2 mM-Cd^{2+}. Holding potential −50 mV. *A* and *B*, sample outward currents evoked by 100 ms depolarizing commands, increasing to +30 mV, plus leak current at −100 mV in *B*. Upper beam, current; lower beam, voltage. Note the reduced current gain in *B*. *C*, repolarizing tail-currents at −50 mV after 100 ms depolarization to −20, −10, 0, +10 and +20 mV. *D*, time course of outward current development at 0 mV command potential, plotted according to eqn. (8) and setting $\gamma = 1$, 2 or 3. *E*, semi-logarithmic time-plots of tail-current decays in *C*. *F*, conductance G_K (◇, μS) at the end of the 100 ms depolarizing commands in *A* and *B* and onset time-constants τ (○, ms), assuming $\gamma = 2$ in eqn. (8), plotted against command potential.

$V_H - V_K$ where V_K is the reversal potential. The latter was estimated for each current response from the ratio of the on- and tail-current amplitudes (see above, p. 548): this is appropriate since the instantaneous current–voltage determined using a series of repolarizing steps of increasing amplitude was linear between +40 and −50 mV in 25 mM-K^+ solution). In this experiment V_K measured in this way shifted from −40 mV after 100 ms depolarization to −20 mV, to −21 mV after depolarizing to +20 mV. The activated conductance G_K attained a value of 2·85 μS at +30 mV, with a threshold around −25 mV (Fig. 14*F*). The maximum conductance $\bar{G}_K$ measured in six cells at command potentials ≥ +30 mV was 2·34 ± S.D. 0·40 μS (i.e. some 30 times greater that $\bar{G}_M$).

I_K kinetics. The sigmoidal on-current time course suggests that I_K in frog sympathetic neurones follows the normal Hodgkin–Huxley kinetic scheme, such that

$$G_K = \bar{G}_K n^\gamma, \tag{6}$$

where $\bar{G}_K$ is the maximum conductance, and hence that I_K develops with time as

$$I_K(t) = I_K(\infty)\left\{1-\exp\left(\frac{-t}{\tau}\right)\right\}^\gamma. \tag{7}$$

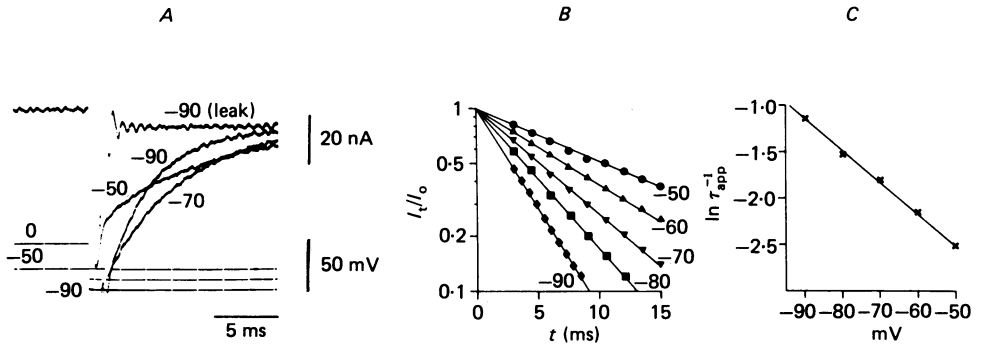

Fig. 15. *A*, tail-currents following a 50 ms depolarizing command to 0 mV, observed at post-pulse potentials of −50, −70 and −90 mV. A single leak-current at −90 mV (i.e. with no depolarizing pre-pulse) is also shown. On-currents are off-scale. *B*, semi-logarithmic plots of tail-current amplitude (normalized to 1 at zero time) against post-pulse time. *C*, logarithm of tail-current reciprocal time constants (τ_{app}^{-1} ms^{-1}) against post-pulse potential. (Experimental conditions as in Fig. 14.)

Fig. 14*D* shows a plot of the logarithmic transformation of eqn. (7):

$$\ln\{1-(I_K(t)/I_K(\infty))^{\gamma^{-1}}\} = -t/\tau, \tag{8}$$

taking $\gamma = 1, 2, 3$. The plot is clearly non-linear at $\gamma = 1$, and linearizes at $\gamma = 2$ or 3. Taking γ (minimum) = 2, the time constant for the on-currents derived from such plots shortened with depolarization from 19 ms at −10 mV to 4 ms at +30 mV (Fig. 14*F*).

In contrast to I_K onset, repolarizing tail-currents showed a simple exponential decay with time (Fig. 14*C* and *E*). Measurements at different repolarizing potentials showed a clear acceleration with increasingly negative repolarizing potentials (Fig. 15). The reciprocal time constant for the current decay diminished exponentially with depolarization, with a slope of −30 mV per *e*-fold depolarization (Fig. 15*C*).

Fig. 16 summarizes kinetic data obtained from five neurones in high-K^+, Ca^{2+}-free solution, with reciprocal time-constants calculated on the assumption that $\gamma = 2$. The rate constants could be fitted by small modifications to Hodgkin–Huxley equations for the squid axon delayed rectifier (Hodgkin & Huxley, 1952) such that

$$\tau_n(V)^{-1} = \alpha_n(V)+\beta_n(V), \tag{9a}$$

$$\alpha_n(V) = \frac{-0{\cdot}0047\ (V+12)}{\exp\left(-(V+12)/12\right)-1} \tag{9b}$$

and

$$\beta_n(V) = \exp\left[\frac{147+V}{-30}\right]. \tag{9c}$$

Thus, I_K kinetics in frog sympathetic neurones resembles that at the nodes of Ranvier of frog myelinated fibres, except that the rate constants for the neuronal currents appear to be about 10 times slower (cf. Frankenhaueser, 1963).

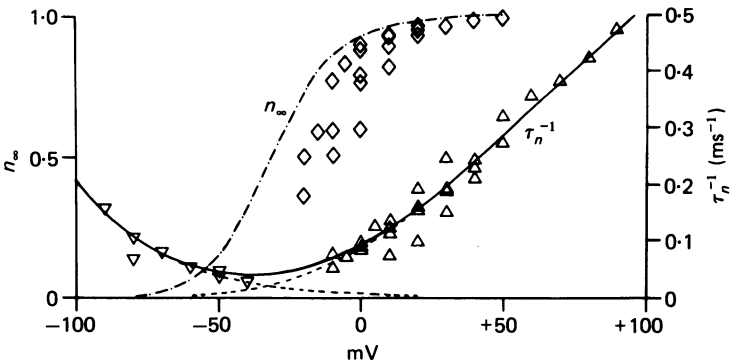

Fig. 16. Summary of I_K kinetic data from five neurones in 25 mM-K^+, 0 Ca^{2+}, 0·2 mM-Cd^{2+} solution. Continuous line, τ_n^{-1} calculated from eqn. (9); points show experimental values for on-currents from plots like that shown in Fig. 14*D* (△) and tail-currents from plots shown in Fig. 15*B* (▽), assuming $\gamma = 2$. Dashed lines show calculated values of α_n and β_n. Dashed and dotted line shows calculated value of n_∞ $(= \alpha_n/(\alpha_n+\beta_n))$; points (◇) show experimental values for n_∞, taking $n_\infty = \sqrt{G_K/\bar{G}_K}$.

Although the fit provided by eqns. (8) and (9) implies that activation and deactivation of I_K in sympathetic neurones in general accords with Hodgkin–Huxley kinetics, the numerical solutions used should be regarded as provisional approximations in view of the restricted data so far available. In evaluating their applicability, the following limitations should be pointed out. (i) Tail-current τ values in the critical range of membrane potential −30 and 0 mV have not yet been obtained, because this voltage range straddles E_K in high-K^+ solution. (ii) Although γ clearly exceeded unity, in no experiment did the plots of eqn. (8) yield a single integer for γ at all command voltages, suggesting some distortion to the onset time course (see below). A value of 2 was chosen as the smallest integer compatible with most of the experimental results. (iii) Although *final* current levels at the end of the command pulses were corrected for shifts in E_K with increasing command pulse amplitude, no correction was attempted for E_K shifts *during* the command pulse since the requisite experimental protocol was too long compared with the useful life-span of the cells. Some modest shift during the pulse was likely, even in elevated $[K^+]$. Thus, as indicated in Fig. 17, the tail-current reversal potential in 48 mM-K^+ shifted from −23 mV after a 10 ms command to +40 mV, to −20 mV after a 70 ms command. Such shifts might distort the onset time-course (Dubois, 1981*a*). (iv) In this scheme, no allowance has been made for I_K inactivation (see below). This may lead to an underestimate of the peak activation of G_K, particularly at modest command potentials where activation is slower and inactivation proportionally more significant (since inactivation was not strongly voltage-dependent), and may explain why the steady-state activation curve predicted from onset and offset kinetics lies to the left of that suggested by the peak currents in Fig. 16. A series resistance will exacerbate this discrepancy by inducing a positive offset between membrane potential and recorded command potential. Taking a 'worst case' illustration, a current of 100 nA at 0 mV command potential into a series resistance of 100 kΩ implies a true membrane potential of −10 mV, not 0 mV.

I_K inactivation. As in several other types of neurone (e.g. squid axon: Ehrenstein & Gilbert, 1966: molluscan neurones: Heyer & Lux, 1976; Aldrich, Getting & Thompson, 1979; frog nodes: Frankenhaueser, 1963; and neuroblastoma cells: Moolenaar & Spector, 1978) I_K declined during prolonged depolarization. This

resulted from a true fall in G_K, rather than from a shift in E_K, since there was a concomitant reduction in the currents evoked by small (−20 mV), brief (10 ms) 'conductance testing' pulses (Fig. 18). In the absence of external Ca^{2+}, the outward current proceeded to complete, or near-complete, inactivation: that is, the residual steady-state current after 0·5–1 min depolarization barely exceeded the 'leak' current evoked by a comparable hyperpolarizing command, and the conductance returned to the resting level. In the presence of external Ca^{2+}, a larger steady-state current persisted, reflecting the Ca^{2+}-generated outward current I_C (see below, and Aldrich *et al.* 1979).

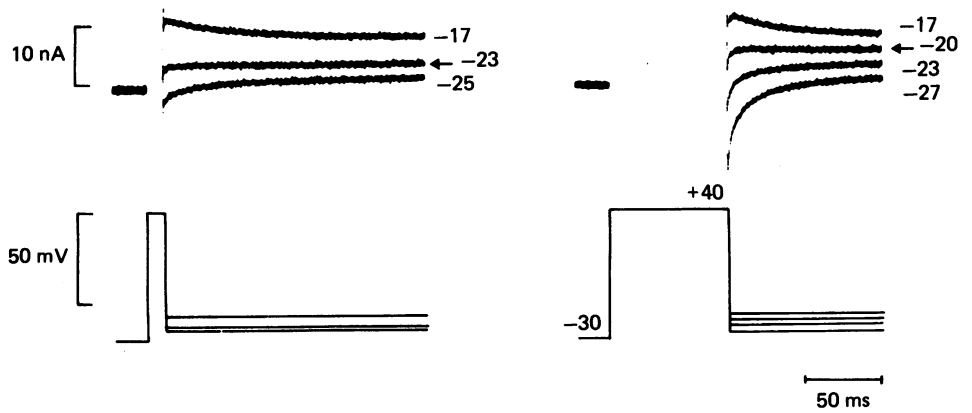

Fig. 17. Tail-currents recorded in a cell in 48 mM-K^+ after 10 and 70 ms depolarizing commands to +40 mV. The command sequence is shown diagrammatically. Note that the tail-current inverted at a repolarizing potential of −23 mV after a 10 ms command and at −20 mV after a 70 ms command.

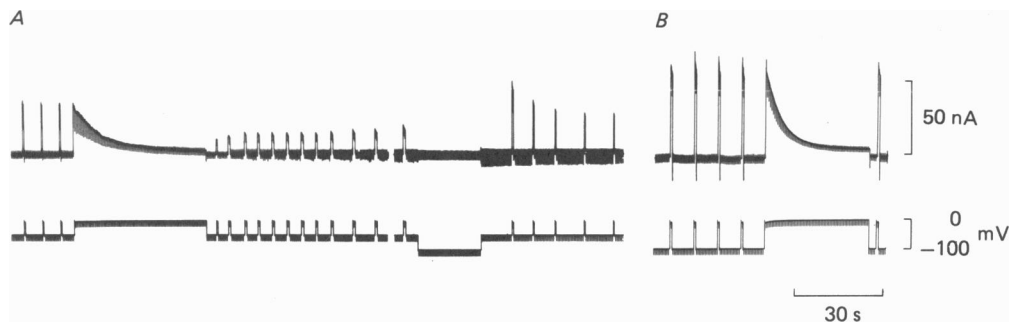

Fig. 18. Inactivation of I_K during prolonged depolarization. A neurone perfused with a Ca^{2+}-free solution (to minimize I_C) was held at −50 mV (in *A*) and subjected to repetitive (2 Hz) hyperpolarizing pulses of 20 mV amplitude, 10 ms width to test conductance. Short (0·5–1 s) depolarizing pulses to 0 mV at ~5 s intervals yielded large constant outward currents, during which the conductance measured by the hyperpolarizing pulses (visible as a thickened current base line) increased about 4 times. During prolonged depolarization to 0 mV, the current and conductance diminished approximately exponentially with time ($\tau \sim 5{\cdot}4$ s), followed by a very slow (and partial) recovery. Interpolation of a 23 s hyperpolarizing command to −100 mV transiently restored the outward current. (A comparable interval at −50 mV did not do this.) In *B* the cell was held at −100 mV and depolarized to 0 mV. The outward current during prolonged depolarization shows similar inactivation ($\tau \sim 4{\cdot}4$ s) but recovered virtually instantaneously on returning to −100 mV.

In both Ca^{2+}-free and Ca^{2+}-solution the decline of I_K toward its steady state followed an approximately exponential time course, with a time constant (τ_{inact}) in the range 4–8 s. There was no very obvious variation of τ_{inact} with membrane potential over the range −10 to +40 mV.

Recovery from inactivation (tested with short pulses applied at ~ 5 s intervals) was very slow and often incomplete, but was accelerated by a short period of hyperpolarization (Fig. 18*A*); recovery at a holding potential of −100 mV was very rapid (Fig. 18*B*).

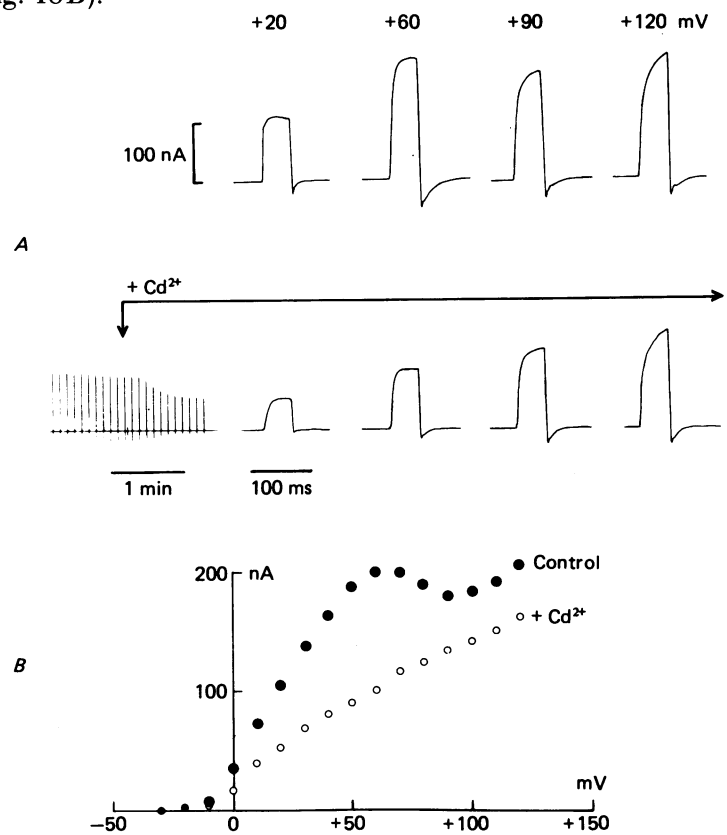

Fig. 19. Effect of Cd^{2+} ions (0·1 mM-$CdCl_2$) on large outward currents evoked by 50 ms depolarizing commands from a holding potential of −30 mV. *A*, sample currents recorded before (upper row) and after (lower row) adding Cd^{2+}. Command potentials are indicated above each pair of current records. The slow time-base records show the effect of adding Cd^{2+} on currents evoked at +20 mV. *B*, graphs show peak currents obtained in the absence (●) and presence (○) of Cd^{2+}. Note that the control current–voltage curve is N-shaped, and that Cd^{2+} abolished the N inflexion.

This form of inactivation, with slow but voltage-sensitive recovery, accords quite closely with the 'slow' inactivation of I_K in molluscan neurones described by Aldrich *et al.* (1979) and attributed to inactivation after channel-opening (Aldrich, 1981). The resumption of inactivation after the hyperpolarization illustrated in Fig. 18 may also imply an equivalent to the 'fast' inactivation from the closed state described by Aldrich *et al.* (1979), though we have as yet no evidence from appropriate paired-pulse experiments to confirm this.

Calcium-activated current (I_C)

In many – but not all – neurones, the current–voltage curve for outward currents activated by 40–100 ms depolarizing commands showed a distinct N shape, peaking between +20 and +60 mV. The N inflexion was reduced or eliminated by perfusing with a Ca^{2+}-free solution, or by adding Cd^{2+} (0·1 mM), Co^{2+} (1 mM) or Mn^{2+} (1 mM) (Fig. 19), which inhibit inward Ca^{2+} currents in these neurones (Adams, 1980). Thus, in such cells, a large proportion of the outward current was probably triggered by Ca^{2+} influx (cf. Meech & Standen, 1975; Heyer & Lux, 1976; Thompson, 1977). Unlike molluscan neurones, however, this Ca^{2+}-dependent current (I_C) was *rapid*, so that inhibition of Ca^{2+} influx *slowed* the outward current over the range −10 to +30 mV. The kinetics of I_C evoked by depolarizing commands and by intracellular Ca^{2+}-injections, are described in some detail elsewhere (Adams, Constanti, Brown & Clark, 1982). For the purpose of the present paper we would merely point out that I_M was not sensitive to external or internal Ca^{2+}, and was not inhibited by Ca^{2+}-channel blockers.

Transient outward current (I_A)

The onset of I_M after repolarization from very hyperpolarized command potentials was preceded by a fast transient outward current (see Fig. 12 for examples). The characteristics of this current (usually examined after suppressing I_M with muscarine) resembled those for the current designated I_A in molluscan neurones by Connor & Stevens (1971) (see also Neher, 1971; Neher & Lux, 1971), and may be summarized as follows:

(*a*) The current was associated with a large increase in membrane conductance, as indicated by the increased amplitude of the instantaneous current steps elicited by a hyperpolarizing command delivered at the peak of the current (Fig. 20*A*).

(*b*) Unlike I_M, the instantaneous current–voltage curve for I_A appeared to show appreciable rectification at membrane potentials more negative than −50 mV (see also Neher, 1971).

(*c*) The activated current reversed in direction on post-pulsing to potentials more negative than −80 to −90 mV; on raising $[K^+]_{out}$ from 2·5 to 25 mM I_A diminished in amplitude and reversed at about −45 mV (Fig. 20*A* and *C*).

(*d*) The threshold command voltage for activating I_A from a strongly hyperpolarized level was about −60 mV (Fig. 21*A*). I_A then increased steeply up to −30 mV; thereafter it could not be followed accurately because of the advent of I_K.

(*e*) Activation of I_A was very rapid (peak < 5 ms at −30 mV) and onset kinetics have not been adequately resolved.

(*f*) Once activated, I_A declined exponentially to zero, with a time constant of about 50 ms at −30 mV. Inactivation was removed by a 1 s pre-pulse to potentials more negative than −70 mV, with half-inactivation at about −110 mV (Fig. 21*B*) and a time-constant for removal of inactivation of ~ 150 ms between −90 and −120 mV. The activation and inactivation curves showed little overlap; hence I_A was completely inactivated at all potentials in its activation range and unlike I_M, did not contribute to the steady membrane current.

(*g*) Activation of I_A following a large hyperpolarizing current pulse induced a clear hyperpolarizing 'notch' on the repolarizing voltage-trajectory recorded under current-

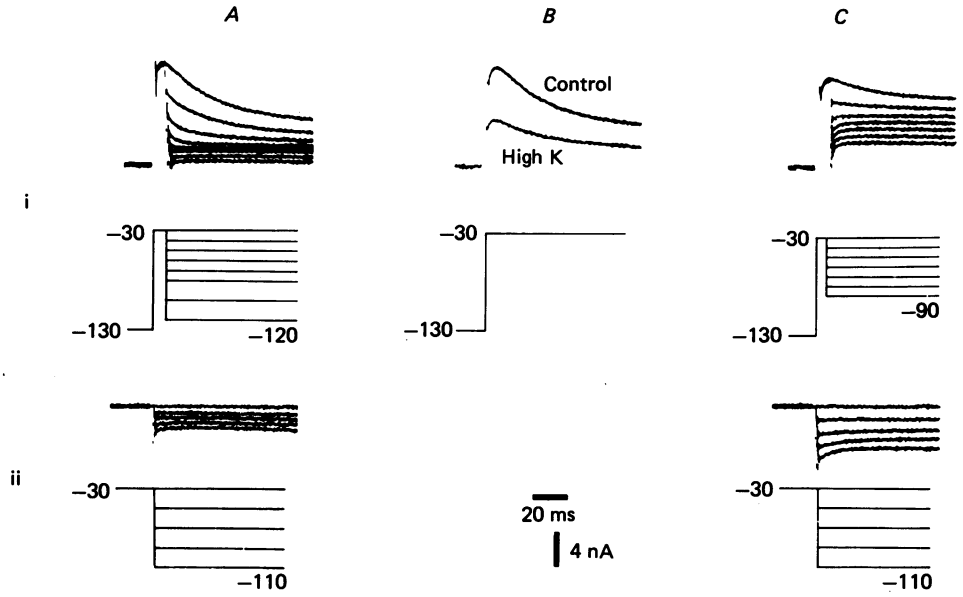

Fig. 20. A-currents evoked in 2·5 and 25 mM-K^+. Records marked i show A-currents elicited by a depolarizing command-pulse to −30 mV after a 1 s pre-pulse to −130 mV to remove I_A inactivation, followed (at 8 ms) by a series of hyperpolarizing post-pulses. Records marked ii show currents after equivalent hyperpolarizing post-pulses from a sustained holding potential of −30 mV, without a pre-pulse (i.e. with I_A fully inactivated). Pulse protocols are indicated schematically below the individual current records. *A*, currents recorded in 2·5 mM-K^+. *B*, effect of raising $[K^+]$ from 2·5 mM (Control) to 25 mM (High K). *C*, family of currents recorded in 25 mM-K^+. Muscarine (10 μM) had been previously added to the Ringer solution to diminish I_M. I_A appears as a transient outward current in records i, following a pre-pulse to remove inactivation. I_A becomes flat or inverts at between −80 and −90 mV post-pulse potential in *A* and reverses between −40 and −50 mV in *B*. The inward relaxations in records ii reflect M-channel closure induced by hyperpolarizing steps from a sustained potential of −30 mV (cf. Fig. 5), and result from incomplete I_M suppression.

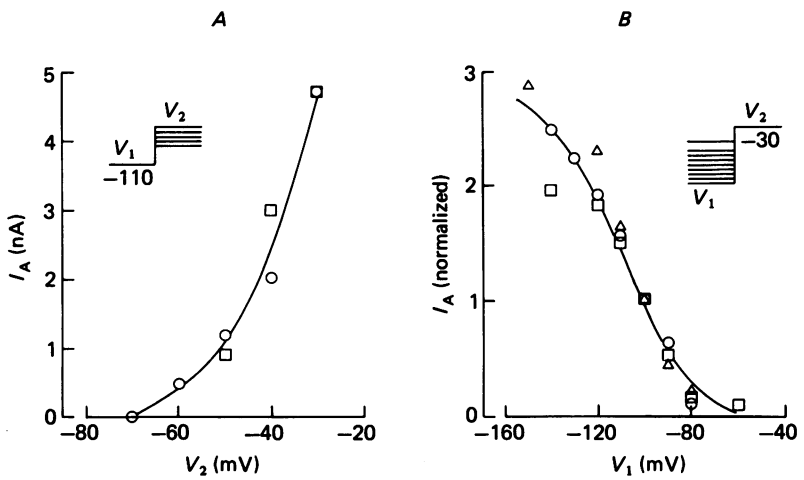

Fig. 21. *A*, activation and *B*, inactivation of I_A. *A*, peak outward currents recorded at increasing post-pulse potentials (V_2) after a pre-pulse to −110 mV for 1 s. *B*, peak outward current recorded at −30 mV post-pulse potential after 0·5–1 s pre-pulses to different potentials (V_1), normalized about the current following a pre-pulse to −100 mV. Each symbol refers to a different experiment in each graph.

clamp, as described by Connor & Stevens (1971), which delayed or totally inhibited the anode-break spike: examples are shown in Fig. 12 and Fig. 24.

One *difference* from the molluscan A-current was that I_A in bullfrog neurones was only weakly inhibited or unaffected by 1 mM-4-aminopyridine.

DISCUSSION

We have identified four distinct K^+ currents in bullfrog sympathetic neurones: (i) a time- and voltage-dependent delayed rectifier current; (ii) an outward current dependent on Ca^{2+}-influx; (iii) a transient current rapidly and completely inactivated at rest; and (iv) a sustained time- and voltage-dependent current activated over a potential range 40 mV negative to that for the delayed rectifier current. The first three currents appear to correspond broadly to those in molluscan neurones previously designated I_K, I_C and I_A (Thompson, 1977); the fourth, which has not been previously described, we have termed the M-current (I_M) because of its sensitivity to muscarinic agonists (see Brown & Adams, 1980).

The underlying conductance for the M-current, G_M, shows a symmetrical activation curve about a half-activation voltage of -35 mV. Both the steady-state activation curve and the voltage dependence of the on- and off- time-constants conform to a very simple model of I_M gating, in which each M-channel may be in either open or shut states (with fixed finite or zero conductance respectively), and in which the state probability is determined by a single gating particle of effective valency $+2{\cdot}5$ moving through the entire membrane electrical field as predicted by a Boltzmann distribution. The near-linear instantaneous current–voltage curves at membrane voltages where G_M is prominent suggests that the individual M-channels do not show pronounced inward or outward rectification, so that the voltage dependence of G_M may be attributed entirely to the change in the proportion of open M-channels.

From a functional viewpoint, I_M occupies a unique position in this hierarchy of K^+ currents because it is the only persistent voltage-sensitive current activated at sub-threshold membrane potentials. At such potentials the time- and voltage-dependent behaviour of the ganglion cell membrane can be modelled using a very simple equivalent circuit comprising a leak pathway and a voltage-sensitive M-pathway (Fig. 22). The conductance of the leak pathway (G_L) is assumed to be voltage-insensitive and to correspond with the slope of the current–voltage curve at very hyperpolarized potentials, when the M-channels are shut: an average value would be about 10 nS. The leak reversal potential V_L is somewhat more conjectural, but must be fairly positive, because pharmacological suppression of I_M leads to membrane depolarization (Brown & Adams, 1980). The value selected (-10 mV) probably represents a composite value determined by the impalement leak and the true passive membrane leak, and – in effect – implies an approximately equal conductance to Na^+ and K^+. (Cl^- does not appear to contribute significantly to the leak conductance, since the slope of the I/V curve was unchanged on replacing external Cl^- with isethionate.) In normal Ringer solution the reversal potential for I_M ($= V_M$) is about -90 mV, and the time- and voltage-dependent behaviour of G_M is described by eqns. (3)–(5).

Taking an average value of the maximal M-conductance ($\bar{G}_M$) as 84 nS, the resting potential predicted by such a model is about –53 mV, in agreement with the better

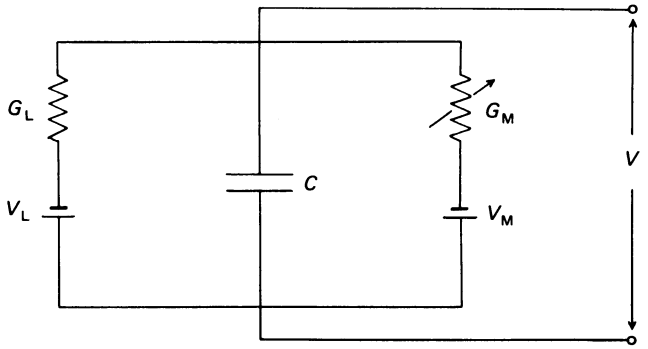

Fig. 22. Equivalent circuit for the resting ganglion cell membrane up to −25 mV. G_L = leak conductance; V_L = reversal potential for leak current; G_M = M-conductance; V_M = reversal potential for M-current; C = capacitance. See text for further details.

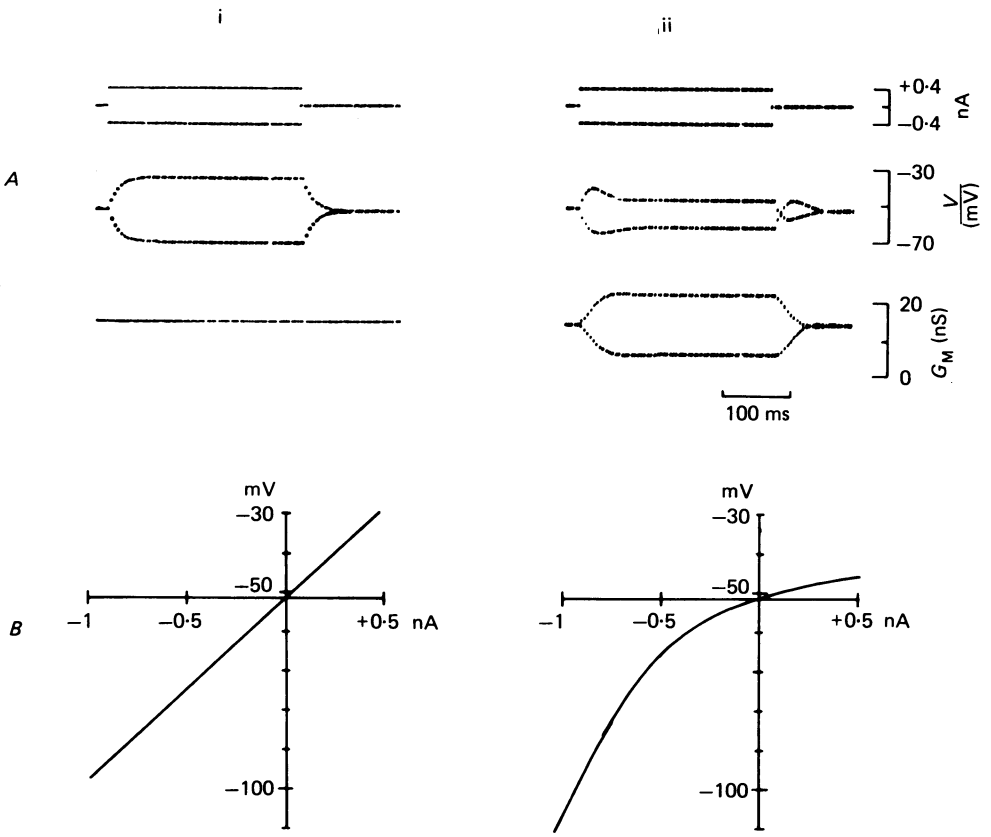

Fig. 23. Predicted responses of the equivalent circuit model in Fig. 22 to current injections (i) with G_M as a fixed conductance and (ii) with G_M as a time- and voltage-sensitive conductance, calculated as described in the Appendix. *A*, time-dependent responses to ±0·4 nA injected current injected for 300 ms. Upper trace, current; middle trace, membrane potential change; lower trace, M-conductance. *B*, membrane potential at the end of the current pulse (i.e. at 300 ms) plotted against current intensity. (A sample of the voltage responses for (ii) is shown in Fig. 24.) See text for parameters. Computational interval Δt = 6 ms.

values recorded experimentally. At this potential some 17 % of the M-channels would be open, conferring an M-conductance of 14 nS and a total membrane conductance of 24 nS (input resistance 42 MΩ).

The responses of such a model cell to current injections were calculated as described in the Appendix, using a value of 0·4 nF for cell capacitance. (This was derived from the time constant of the voltage excursion during large hyperpolarizing current injections, sufficient to turn off I_M rapidly and completely: it is equivalent to ~ 8 μF/cm^2 for a 20 μm radius cell, in agreement with the calculation of Nishi &

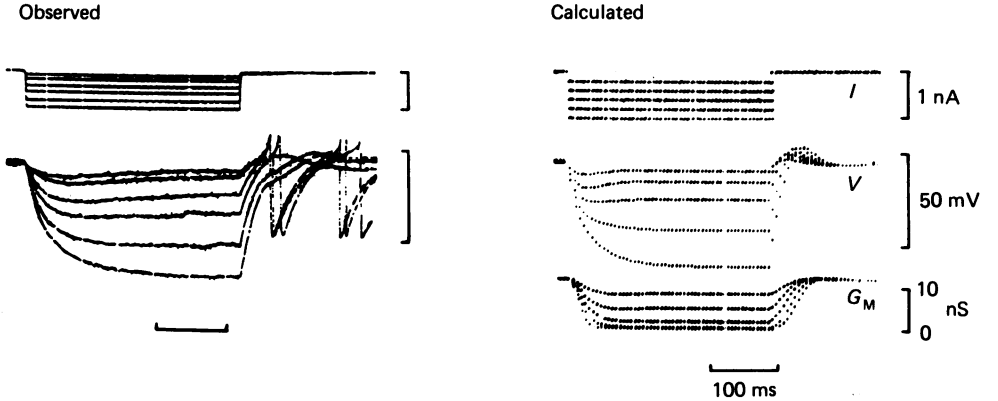

Fig. 24. Comparison of experimentally observed voltage deflexions produced by a series of increasing hyperpolarizing current injections (left panel) with those predicted from the equivalent circuit shown in Fig. 22 with a voltage-sensitive G_M (right panel). (Note: in this cell responses were recorded using the single micro-electrode sample-and-hold method previously described (Constanti & Brown, 1981), to minimize impalement leaks. Note also that the observed off-trajectories following the cessation of small hyperpolarizing currents show the rebound depolarization predicted, but after large currents are obscured by a hyperpolarizing 'notch' due to activation of the transient outward current I_A: see text).

Koketsu (1960).) The right-hand panel of Fig. 23 shows the predicted voltage deflexions following injections of depolarizing and hyperpolarizing current. Depolarizing current rapidly increases G_M and this induces a secondary outward current and secondary hyperpolarization; conversely, hyperpolarizing current deactivates G_M, producing a secondary inward current. In consequence the steady-state current–voltage curve shows pronounced outward rectification, in the manner illustrated in Fig. 23*B*. The influence conferred by the voltage sensitivity of G_M in limiting the voltage excursions is clearly shown by reference to the left-hand panel of Fig. 23, in which G_M is replaced by an equivalent (14 nS) *fixed* K^+ conductance. The steady-state voltage deflexions produced by ±0·4 nA current are approximately twice as large and (of course) the I/V curve does not show rectification.

The form of the voltage trajectories in Fig. 23*A*, and the rectification of the I/V curve in Fig. 23*B*, clearly resemble those previously illustrated in Figs. 12 and 13. The agreement between predicted and observed responses is particularly striking for hyperpolarizing current injections, as shown in Fig. 24. This suggests that the equivalent circuit model in Fig. 22 is sufficient to provide an essentially correct description of the 'subthreshold' behaviour of the ganglion cell membrane.

Another helpful way of illustrating the 'stabilizing' effect of I_M on the steady-state membrane potential is to calculate (from the equivalent circuit in Fig. 22) what would happen to the resting potential when the leak conductance is increased. This is shown in Fig. 25. If the resting M-conductance were a fixed (voltage-insensitive) conductance of 14 nS, a 5-fold increase in leak conductance (as might be induced by an excitatory transmitter) would depolarize the cell by about 27 mV (broken line in Fig. 25). Conferment of voltage sensitivity on G_M reduces this depolarization to less than half (12 mV: continuous line in Fig. 25).

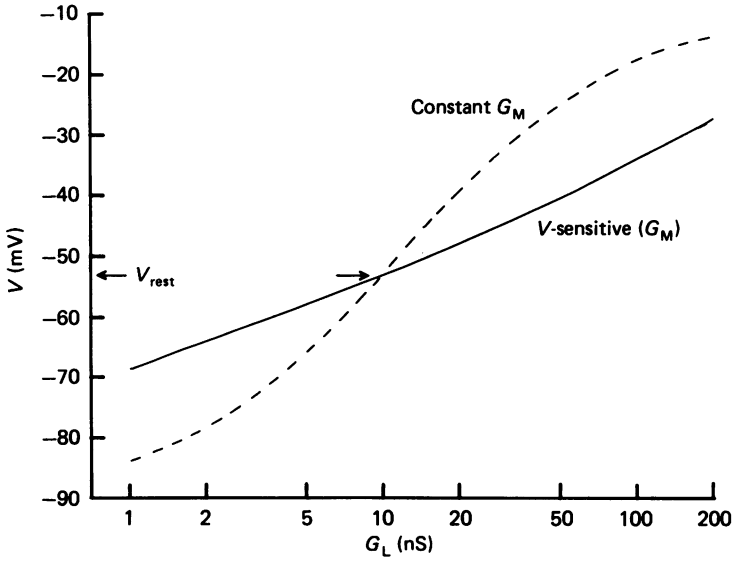

Fig. 25. Variation of resting potential (V) with leak conductance (G_L) in the ganglion cell equivalent circuit shown in Fig. 22, calculated as described in the Appendix. The solid curve shows the membrane potential predicted for a voltage-sensitive M-conductance (G_M) behaving as shown in eqn. (3) with a maximal value ($\bar{G}_M$) of 84 nS. The dashed curve shows the corresponding membrane potential when G_M is replaced by a voltage-insensitive conductance with a constant value of 14 nS (equal to the value of G_M at rest potential $V_{rest}(=-53$ mV), when $G_L = 10$ nS). Other constants: $V_M(\approx V_K) = -90$ mV, $V_L = -10$ mV.

Thus, I_M would be expected to exert a strong 'potential clamping' effect on the cell membrane when attempts are made to displace it from rest potential by such procedures as injecting current or changing the membrane conductance. This is confirmed by the striking increase in excitability when I_M is suppressed pharmacologically (Brown, Adams & Constanti, 1982). (This point will be explored in more detail in a subsequent publication.) I_M has now been confirmed in frog neurones (McDermott & Weight, 1980; Akasu, 1981), and has also been detected in voltage-clamped mammalian sympathetic neurones (Constanti & Brown, 1981; Kobayashi, Hashiguchi, Tosaka & Mochida, 1981) and in some mammalian central neurones (hippocampal pyramidal cells: Adams, Brown & Halliwell, 1981; mouse spinal neurones: Nowak & Macdonald, 1981; guinea-pig olfactory neurones: A. Constanti & M. Galvan, unpublished observations). This suggests that the M-current might provide a rather widespread and fundamental mechanism for controlling neuronal excitability.

APPENDIX

Computer simulation of M-current kinetics

Program MKIN was written in FOCAL-12 using a PDP-12 computer (Digital Equipment Corp.). The aim of the program was to stimulate the time course of the electrotonic potential in response to a rectangular current step injected into a hypothetical spherical cell represented by a conventional parallel resistor/capacitor network (see Fig. 22).

The only conductances operating in the membrane were assumed to be a voltage and time-independent 'leak' conductance (G_L). and a voltage/time-dependent M-channel conductance (G_M). The net membrane current (I_m) flowing across the cell membrane at any instant would then be given by,

$$I_m = I_C + \bar{G}_M y_M(t)(V - V_M) + \bar{G}_L(V - V_L), \tag{A 1}$$

where $I_C = C.\ dV/dt$ (capacity current), $\bar{G}_M$, $\bar{G}_L$ are the maximum activatable M channel or leak channel conductances respectively, V_M and V_L the respective reversal potentials and $y_M(t)$ the instantaneous fraction of active M-channels.

The voltage and time dependence of the M-channels were assumed to obey simple first-order Hodgkin–Huxley-type kinetics such that

$$\frac{dy_M}{dt} = \alpha_M - y_M(t)\ \{\alpha_M + \beta_M\}, \tag{A 2}$$

where α_M, β_M are the channel opening and closing rate constants respectively.

According to Boltzmann's principle, the fraction of open M-channels in the steady state ($t = \infty$) would be governed by the membrane distribution of a gating particle of effective valency z so that

$$y_M(\infty) = \left\{1 + \exp\left[\frac{ze}{kT}(V_0 - V)\right]\right\}^{-1} \tag{A 3}$$

and,

$$\begin{Bmatrix}\alpha_M \\ \beta_M\end{Bmatrix} = \begin{Bmatrix}\alpha_M(0) \\ \beta_M(0)\end{Bmatrix} \left\{\exp\left[(\pm)\frac{ze}{2kT}(V - V_0)\right]\right\}, \tag{A 4}$$

where V_0 is the half-activation voltage, $\alpha_M(0)$, $\beta_M(0)$ the corresponding rate constants at V_0 and kT/e ($= RT/F$) have their usual meaning (= 25 mV at 22 °C).

Using eqns. (A 1) and (A 3), the initial part of the programme calculated the effective 'resting' potential of the cell (V_{rest}) in the steady state (i.e. $dV/dt = 0$, $I_m = 0$). This required finding a value of V such that

$$f(V) = \{y_M(\infty)\,\bar{G}_M(V - V_K) + \bar{G}_L(V - V_L)\} = 0.$$

With the modified Newton–Raphson iteration method (Tranter, 1957), if a root of the equation $f(V) = 0$ is known to lie between $V = V_e$ and $V = V_e + \phi$, where ϕ is a small increment, then a better approximation V_e' may be obtained by calculating

$$V_e' = \left\{V_e - \frac{\Delta . f(V_e)}{f(V_e + \phi) - f(V_e)}\right\}, \tag{A 5}$$

where Δ is the difference between the upper and lower estimates (initially = ϕ). The process was repeated (replacing V_e by V_e' as the *lower* estimate and recalculating Δ)

until the absolute difference between two successive approximations was $< 0{\cdot}01$. If the initial lower estimate V_e was close to the true root, the calculation converged rapidly in less than thirty iterations. If V_e was not close, the successive estimates of V_e' 'oscillated' between two stable values without converging. The value of ϕ was not apparently crucial to the success of the computation and was typically set $= -0{\cdot}01$ mV.

Effects of current injection

The calculated value of V_{rest} was used to obtain the initial value of $y_M(\infty)$ (eqn. (A 3)) before the current step. These resting values of V_{rest} and $y_M(\infty)$ were then plotted at time intervals Δt to provide a base line for the pre-step duration. Immediately after application of the current step (I), I_m in eqn. (A 1) was set $= I$ and I_C calculated (initially, $V = V_{rest}$). For a small increment in time Δt, the increment in membrane potential could be obtained from

$$\Delta V = \Delta t \,.\, I_c/C. \tag{A 6}$$

The increment in the M-parameter (Δy_M) had now to be calculated at the new membrane potential $V_{rest}+\Delta V$. By rearranging eqn. (A 2), the instantaneous value of $y_M(y_M(t))$ could be expressed as a function of time thus:

$$y_M(t) = f(t) = \{y_M(\infty) - \tau_M \,.\, \mathrm{d}y_M/\mathrm{d}t\}, \tag{A 7}$$

where $\tau_M = (\alpha_M+\beta_M)^{-1}$ and $y_M(\infty) = \alpha_M/(\alpha_M+\beta_M)$. For a given function $f(t)$, the Taylor expansion of the function $f(t+\Delta t)$ gives

$$f(t+\Delta t) \approx f(t) + \Delta t \,.\, f'(t),$$

where $f'(t)$ is the first differential derivative (cf. Palti, 1971). When applied to eqn. (A 7),

$$y_M(t+\Delta t) \approx y_M(t) + \Delta t \,\{\alpha_M' - y_M(t)\,[\alpha_M'+\beta_M']\}$$

and since $\alpha_M' = y_M'(\infty)/\tau_M'$,

$$\Delta y_M \approx \frac{\Delta t}{\tau_M'}\{y_M'(\infty) - y_M(t)\}. \tag{A 8}$$

The increment Δy_M was thus obtained by calculating τ_M' and $y_M'(\infty)$ pertaining to the *new* membrane potential ($V_{rest}+\Delta V$), with $y_M(t)$ referring to the immediately previous instantaneous value. After incrementing the initial value of $y_M(\infty)$ by Δy_M, eqns. (A 1), (A 6) and (A 8) were re-applied to find new increments in V and y_M respectively, and the process continued for the duration of the current step. On cessation of the step, I_M was set $= 0$ in eqn. (A 1) and the calculation of V and y_M continued for the post-pulse period. During and after the current pulse, the instantaneous values of V and y_M were plotted for each time increment Δt(1–6 ms).

Thus, after initial entry of appropriate values for V_K, V_L, C, $\bar{G}_M$, $\bar{G}_L$, I and Δt, the program computed the 'resting' potential then plotted the shape of the electrotonic potential and underlying changes in y_M during and after the injection of a current step.

This study was aided by NIH grants NS 14920 and 14986 to P.R.A. and by grants from the Wellcome Trust and the Medical Research Council to D.A.B. and A.C. P.R.A. is a Sloane Fellow.

REFERENCES

ADAMS, P. R. (1980). The calcium current of a vertebrate neuron. *Fedn Proc.* **39**, 282.

ADAMS, P. R. & BROWN, D. A. (1980). Ionic basis of the slow excitatory post-synaptic potential in voltage clamped bullfrog sympathetic neurones. *J. Physiol.* **303**, 66*P*.

ADAMS, P. R., BROWN, D. A. & HALLIWELL, J. V. (1981). Cholinergic regulation of M-current in hippocampal pyramidal cells. *J. Physiol.* **317**, 29–30*P*.

ADAMS, P. R., CONSTANTI, A., BROWN, D. A. & CLARK, R. B. (1982). Intracellular Ca^{2+} activates a fast voltage-sensitive K^+ current in vertebrate sympathetic neurones. *Nature, Lond.* **296**, 746–749.

ADAMS, P. R. & HALLIWELL, J. V. (1982). A hyperpolarization-induced inward current in hippocampal pyramidal cells. *J. Physiol.* **324**, 62–63*P*.

AKASU, T. (1981). Voltage-clamp analysis of muscarinic effects on action potentials in sympathetic ganglion cells of bullfrogs. *Neurosci. Lett.* suppl. **6**, S. 59.

ALDRICH, R. W. (1981). Inactivation of voltage-gated delayed potassium current in molluscan neurons. *Biophys. J.* **36**, 519–532.

ALDRICH, R. W. Jr., GETTING, P. A. & THOMPSON, S. H. (1979). Inactivation of delayed outward current in molluscan neurone somata. *J. Physiol.* **291**, 507–530.

BARRETT, E. F., BARRETT, J. N. & CRILL, W. E. (1980). Voltage-sensitive outward currents in cat motoneurones. *J. Physiol.* **304**, 251–276.

BLACKMAN, J. G., GINSBORG, B. L. & RAY, C. (1963). Synaptic transmission in the sympathetic ganglion of the frog. *J. Physiol.* **167**, 355–373.

BROWN, D. A. & ADAMS, P. R. (1979). Muscarinic modification of voltage-sensitive currents in sympathetic neurons. *Neurosci. Abstr.* **5**, 585.

BROWN, D. A. & ADAMS, P. R. (1980). Muscarinic suppression of a novel voltage-sensitive K^+-current in a vertebrate neurone. *Nature, Lond.* **283**, 673–676.

BROWN, D. A., ADAMS, P. R. & CONSTANTI, A. (1981). Slow cholinergic and peptidergic transmission in sympathetic ganglia. *Fedn Proc.* **40**, 2625–2630.

BROWN, D. A., ADAMS, P. R. & CONSTANTI, A. (1982). Voltage-sensitive K-currents in sympathetic neurones and their modification by neurotransmitters. *J. aut. nerv. Syst.* (in the Press).

BROWN, H. F., CLARK, A. & NOBLE, S. J. (1976). Analysis of pacemaker and repolarization currents in frog atrial muscle. *J. Physiol.* **258**, 547–577.

BROWN, H. F. & DIFRANCESCO, D. (1980). Voltage-clamp investigations of membrane currents underlying pace-maker activity in rabbit sino-atrial node. *J. Physiol.* **308**, 331–351.

CONNOR, J. A. & STEVENS, C. F. (1971). Voltage-clamp studies of a transient outward membrane current in gastropod neural somata. *J. Physiol.* **213**, 21–30.

CONSTANTI, A. & BROWN, D. A. (1981). M-currents in voltage-clamped mammalian sympathetic neurones. *Neurosci. Lett.* **24**, 289–294.

DIFRANCESCO, D., NOMA, A. & TRAUTWEIN, W. (1979). Kinetics and magnitude of the time-dependent potassium current in rabbit sino atrial node. *Pflügers Arch.* **381**, 271–279.

DUBOIS, J. M. (1981*a*). Simultaneous changes in the equilibrium potential and potassium conductance in voltage clamped Ranvier nodes in the frog. *J. Physiol.* **318**, 279–295.

DUBOIS, J. M. (1981*b*). Evidence for the existence of three types of potassium channels in the frog Ranvier node membrane. *J. Physiol.* **318**, 297–316.

DUBOIS, J. M. & BERGMAN, C. (1975). Potassium accumulation in the perinodal space of frog myelinated axons. *Pflügers Arch.* **358**, 111–124.

EHRENSTEIN, G., BLUMENTHAL, R., LATORRE, R. & LECAR, H. (1974). Kinetics of the opening and closing of individual excitability-inducing material channels in a lipid bilayer. *J. gen. Physiol.* **63**, 707–721.

EHRENSTEIN, G. & GILBERT, D. L. (1966). Slow changes of potassium permeability in the squid giant axon. *Biophys. J.* **6**, 553–566.

FRANKENHAEUSER, B. (1963). A quantitative description of potassium currents in myelinated nerve fibres of *Xenopus laevis*. *J. Physiol.* **169**, 424–430.

FRANKENHAEUSER, B. & HODGKIN, A. L. (1956). The after-effects of impulses in the giant nerve fibres of *Loligo*. *J. Physiol.* **131**, 341–376.

HEYER, C. B. & LUX, H. D. (1976). Control of the delayed outward potassium currents in bursting pace-maker neurones of the snail, *Helix pomatia*. *J. Physiol.* **262**, 349–382.

HODGKIN, A. L. & HUXLEY, A. F. (1952). A quantitative description of membrane current and its application to conduction and excitation in nerve. *J. Physiol.* **117**, 500–544.

HUNT, C. C. & NELSON, P. G. (1965). Structural and functional changes in the frog sympathetic ganglion following cutting of the presynaptic nerve fibres. *J. Physiol.* **177**, 1–20.

KOBAYASHI, H., HASHIGUCHI, T., TOSAKA, T. & MOCHIDA, S. (1981). Muscarinic antagonism of a persistent outward current in sympathetic neurons of rabbits and its partial contribution to the generation of the slow epsp. *Neurosci. Lett.* suppl. **6**, S. 64.

LEE, K. S., WEEKS, T. A., KAO, R. L., AKAIKE, N. & BROWN, A. M. (1979). Sodium current in single heart muscle cells. *Nature, Lond.* **278**, 269–271.

MACDERMOTT, A. B. & WEIGHT, F. F. (1980). The pharmacological blockade of potassium conductance in voltage-clamped bullfrog sympathetic neurons. *Fedn Proc.* **39**, 2074.

MAUGHAM, D. W. (1973). Some effects of prolonged polarization on membrane currents in bullfrog atrial muscle. *J. Membrane Biol.* **11**, 331–352.

MEECH, R. W. & STANDEN, N. B. (1975). Potassium activation of *Helix aspersa* neurones under voltage clamp: a component mediated by calcium influx. *J. Physiol.* **249**, 211–239.

MOOLENAAR, W. H. & SPECTOR, I. (1978). Ionic currents in cultured mouse neuroblastoma cells under voltage-clamp conditions. *J. Physiol.* **278**, 265–286.

NEHER, E. (1971). Two fast transient current components during voltage clamp on snail neurons. *J. gen. Physiol.* **58**, 36–53.

NEHER, E. & LUX, H. D. (1971). Properties of somatic membrane patches of snail neurons under voltage clamp. *Pflügers Arch.* **322**, 35–38.

NISHI, S. & KOKETSU, K. (1960). Electrical properties and activities of single sympathetic neurons in frogs. *J. cell. comp. Physiol.* **55**, 15–30.

NISHI, S., SOEDA, H. & KOKETSU, K. (1965). Studies on sympathetic B and C neurons and patterns of preganglionic innervation. *J. cell. comp. Physiol.* **66**, 19–32.

NOBLE, S. J. (1976). Potassium accumulation and depletion in frog atrial muscle. *J. Physiol.* **258**, 579–613.

NOBLE, D. & TSIEN, R. W. (1968). The kinetic and rectifier properties of the slow potassium current in cardiac Purkinje fibre. *J. Physiol.* **195**, 185–214.

NOMA, A. & IRISAWA, H. (1976). Membrane currents in the rabbit sino atrial node cell as studied by double microelectrode method. *Pflügers Arch.* **364**, 45–52.

NOWAK, L. M. & MACDONALD, R. L. (1981). DL-muscarine decreases a potassium conductance to depolarize mammalian spinal cord neurons in cell culture. *Neurosci. Abstr.* **7**, 725.

PALTI, Y. (1971). Digital computer reconstruction of axon membrane action potential. In *Biophysics and Physiology of Excitable Membranes*, ed. ADELMAN, W. J., JR., pp. 215–222. New York: Van Nostrand Reinhold.

THOMPSON, S. H. (1977). Three pharmacologically distinct potassium channels in molluscan neurones. *J. Physiol.* **265**, 465–488.

TOSAKA, T., CHICHUBU, S. & LIBET, B. (1968). Intracellular analysis of slow inhibitory and excitatory postsynaptic potentials in sympathetic ganglia of the frog. *J. Neurophysiol.* **31**, 396–409.

TRANTER, C. J. (1957). *Techniques of Mathematical Analysis*, pp. 128–129. London: English Universities Press.

WEITSEN, H. A. & WEIGHT, F. F. (1977). Synaptic innervation of sympathetic ganglion cells in the bullfrog. *Brain Res.* **128**, 197–211.

YANAGIHARA, K. & IRISAWA, H. (1980). Inward current activated during hyperpolarization in the rabbit sino atrial node. *Pflügers Arch.* **385**, 11–19.